DESIGN AND PRODUCTION OF ANTIREFLECTION COATING FOR Ge, ZnSe AND ZnS IN 8-12 MICROMETER WAVELENGTH REGION

A THESIS SUBMITTED TO

THE GRADUATE SCHOOL OF NATURAL AND APPLIED SCIENCES

OF

THE MIDDLE EAST TECHNICAL UNIVERSITY

BY

BEGÜM ÜÇER

IN PARTIAL FULFILLMENT OF THE REQUIREMENTS

FOR

THE DEGREE OF MASTER OF SCIENCE

IN

PHYSICS

DECEMBER 2009

Approval of the thesis:

DESIGN AND PRODUCTION OF ANTIREFLECTION COATING FOR Ge, ZnSe AND ZnS IN 8-12 MICROMETER WAVELENGTH REGION

submitted by **BEGÜM ÜÇER** in partial fulfillment of the requirements for the degree of **Master of Science in Physics Department, Middle East Technical University** by,

Prof. Dr. Canan Özgen _____
Dean, Graduate School of **Natural and Applied Sciences**

Prof. Dr. Sinan Bilikmen _____
Head of Department, **Physics**

Prof.Dr. Mehmet Parlak
Supervisor, **Physics Dept., METU** _____

Examining Committee Members:

Prof. Dr. İbrahim Günal _____
Physics Dept., METU

Prof. Dr. Mehmet Parlak _____
Physics Dept., METU

Prof. Dr. Nizami Hasanli _____
Physics Dept., METU

Assoc. Prof. Dr. Akif Esendemir _____
Physics Dept., METU

Dr. Yavuz Aka _____
Roketsan Inc.

Date: December 2009

I hereby declare that all information in this document has been obtained and presented in accordance with academic rules and ethical conduct. I also declare that, as required by these rules and conduct, I have fully cited and referenced all material and results that are not original to this work.

Name, Last name: Begüm Üçer

Signature:

ABSTRACT

DESIGN AND PRODUCTION OF ANTIREFLECTION COATING FOR Ge, ZnSe AND ZnS IN 8-12 MICROMETER WAVELENGTH REGION

Üçer Begüm

M.S., Department of Physics

Supervisor: Prof. Dr. Mehmet Parlak

December 2009, 72 pages

This thesis describes the works done during the design and deposition process of the antireflection coating for the materials commonly used as refractive optical elements in thermal imaging systems. These coatings are quite necessary to reduce reflection losses from the surface of the optics and stray light that directly affects the image quality.

Germanium, zinc sulfide and zinc selenide were used as substrate material and their optical properties were investigated with infrared ellipsometry and FTIR. Antireflection coatings for each material operating in 8-12 μm range were designed with Needle Synthesis Technique. In order to shorten the optimization time, commercial software; "The Essential Macleod" was used. In order to reduce the reflectance losses multilayer structure was used in the coating design, and zinc selenide and lead telluride were used as low and high index materials.

In this study the necessary theoretical background and common deposition techniques are reviewed. Samples were produced using the magnetron sputtering. To optimize the

thicknesses of the deposited layers, growth period and rate was controlled. Thicknesses of the samples, following to the deposition were also measured by thickness profilometer.

A 3-layer coating, PbTe/ZnSe/PbTe, on ZnS and 2-layer coating PbTe/ZnS on Ge having more than 90% transmittance in 9.7-10.3 μm wavelength region have been successfully produced. Although, the measured range for 3 and 2- layer coating is narrower than the aimed one, it has been shown that, the method developed in this thesis would yield AR-coatings with broader spectral response if a system having better control on deposition parameters is used. For example, our design and optimization work has suggested that a 7-layer AR coating on germanium, with alternating high and low index layers is expected to give transmittance value greater than 93% in the studied wavelength region.

Keywords: Antireflection Coating, Infrared, Sputtering, Needle Method, The Essential Macleod.

ÖZ

Ge,ZnSe VE ZnS İÇİN 8-12 MİKROMETRE DALGA BOYU ARALIĞINDA YANSIMA ÖNLEYİCİ KAPLAMA TASARIMI VE ÜRETİMİ

Üçer Begüm

Yüksek Lisans, Fizik Bölümü

Tez Yöneticisi: Prof. Dr. Mehmet Parlak

Aralık 2009, 72 Sayfa

Bu tez termal görüntüleme sistemlerinde yaygın olarak kırıcı optik eleman olarak kullanılan malzemeler üzerine yapılan yansımayı önleyici kaplamaların tasarım ve uygulama sürecini anlatmaktadır. Bu kaplamalar, kırıcı optik elemanların yüzeyinden yansımaların ve sistem içindeki gereksiz ışımaların azaltılması için gereklidir.

Germanyum, çinko sülfit ve çinko selenit altlık malzemeleri olarak kullanılmış ve optik özellikleri kızılötesi elipsometre ve Fourier dönüşümü kızılötesi spektrometresi ile belirlenmiştir. Her bir malzeme için 8-12μm aralığında çalışan yansıma önleyici kaplamalar Needle sentez metodu ile tasarlanmıştır. Optimizasyon sürecini kısaltmak amacıyla "The Essential Macleod" isimli ticari yazılım kullanılmıştır. Yansıma kayıplarını azaltmak için kaplama tasarımında çok katmanlı bir yapı kullanılmıştır. Bunu yaratmak için çinko selenit ve kurşun tellür düşük ve yüksek kırıcılık indisli malzemeler olarak kullanılmıştır.

Bu tezde gerekli teorik altyapı bilgisi ve yaygın olarak kullanılan kaplama teknikleri gözden geçirilmiştir. Örnekler magnetron ile saçtırma yöntemiyle üretilmiştir. Büyütülen katmanların kalınlığını optimize etmek için büyütme süresi ve değişimi kontrol edilmiş, sonrasında ise kalınlık profilometresi ile örnek kalınlıkları ölçülmüştür.

9.7-10.3 μm dalga boyu aralığında geçirgenliği % 90'ın üzerinde olan, ZnS üzerine üç katlı PbTe/ZnSe/PbTe ve Ge üzerinede iki katlı PbTe/ZnS kaplamalaı başarı ile üretilmiştir. Her ne kadar üretilen 2 ve 3 katmanlı kaplamanın optimizasyon aralığı hedeflenen aralıktan dar olsa da, bu tezde geliştirilen metodun kaplama parametreleri üzerinde daha iyi kontrol sağlayan bir kaplama sistemi kullanıldığında, daha geniş band aralığında spektral tepkisi olan yansıma önleyici kaplamalar vereceği gösterilmiştir. Örneğin germenyum üzerine sırası

ile yüksek ve düşük kırıcılık indisli katmanlarla yedi katlı AR kaplamanın % 93 ün üzerinde geçirgenlik vermesi beklenmektedir.

Anahtar Kelimeler: Yansımayı Önleyici Kaplama, Kızılötesi, Saçtırma, Needle Metodu, The Essential Macleod.

To my mom, Asuman…

ACKNOWLEDGEMENTS

I would like to thank my parents Asuman and Yavuz for their love and support throughout my life. I also wish to thank my brother Burak for being in my life.

I wish to express my appreciation to Prof. Dr. İbrahim Günal for taking care of everything in my life.

I am grateful for my supervisor Prof. Dr. Mehmet Parlak for his endless patient. And also, I would like to thank my boss Dr. Kazım Küçükturhan for believing me and supporting this work.

I also would like to thank my boyfriend Eren for cleaning my house and feeding me during thesis process. My thanks also go to my lovely dog Odin for always making me happy.

And Finally, I would like to thank my lovely friends Nilgün and Nejat Lüleci for being such a perfect human beings.

TABLE OF CONTENTS

LIST OF TABLES

TABLE

LIST OF FIGURES

FIGURES

LIST OF SYMBOLS AND ABBREVATIONS

APCVD	Atmospheric Pressure Chemical Vapor Deposition
BPSG	Borophosphosilicate Glass
CVD	Chemical Vapor Deposition
D	Dektak
E_g	Band Gap
FT	Fourier Transform
FTIR	Fourier Transform Infrared spectrometer
IC	Integrated Circuit
IR	Infrared
LPCVD	Low Pressure Chemical Vapor Deposition
PECVD	Plasma-Enhanced Chemical Vapor Deposition
PVD	Physical Vapor Deposition
r	Reflection Coefficient
RF	Radio Frequency
t	Transmission Coefficient
TE	Transverse Electric
TM	Transverse Magnetic
TMo	Thickness Monitor
UV	Ultra Violet

CHAPTER 1

INRODUCTION

Thermal imaging systems have great importance in today's world. These devices are widely used in air and ground surveillance systems and missile seekers. For instance, an anti-tank missile seeker operating at 8-12 μm range has to detect a stationary tank many kilometers away [1]. In other words, this seeker has a small amount of flux coming from that tank which means any losses arising from the optics in the seeker should be reduced. In addition to the intensity loss due to reflection, stray light, which reduces the image contrast, arises from these reflections. In an imaging system, refractive optical elements, lenses, should be used to obtain an appropriate image. Germanium is the one of the most popular lens material because of its optical properties [2]. However, its high refractive index makes it quite reflective resulting from the huge refractive index difference at the air-to material interface. To generalize, not only germanium but also other materials used in 8-12 μm range have large refractive indexes which make anti-reflection coatings inevitable in thermal imaging systems.

Coating the surface of the substrate with a transparent material having the suitable optical path difference minimizes the reflections. Such coatings are called "anti-reflection coatings". The physics behind it is the interference. These coatings are designed so that the reflected light forms a destructive interference whereas the transmitted one forms a constructive interference. Destructive interference of the reflected light prevents the stray light in the system while the constructive interference increases the transmitted light intensity. The most primitive form of such coatings is the single layer anti-reflection coating. However, this works only for a single wavelength. To achieve a low level reflection losses over a broad band multilayer coatings of alternating high and low index materials are needed. Unlike the availability of the materials used in the visible region, there is limited number of coating materials with suitable refractive index and transparent in 8-12 μm range. In this work PbTe and ZnSe are used as high and low index material, respectively.

The main idea behind the multilayer anti-reflecting system design is to convert a graded index profile with desired reflectivity into a more producible multilayer coating with same spectral response in the corresponding wavelength region. Many optimization techniques [3] can be used to improve system performance while doing this conversion. Although some design and optimization approach will be given in this work, final optimizations and system evaluation will be carried out with the help of commercial computer program called Essential Macleod to fasten the process.

In the present work, we have planned to produce a multilayer anti reflecting structure to be used in a thermal imaging system by using germanium, zinc sulfide or zinc selenide substrates. The design and optimization as well as the production and characterization are the main items presented here.

In chapter two, all the necessary background information about materials to be used, the optics of the multilayer structure, design and optimization are given. The deposition techniques together with the thickness control are also discussed.

All the experimental work performed to produce the multilayer and to characterize them together with the methodology are given in details in chapter 3. This chapter also includes the computer aided design process.

Chapter four summarizes the results and their discussions while the conclusion is presented in Chapter 5.

CHAPTER 2

BACKGROUND INFORMATION

2.1. Substrate Layer and Layer Materials

2.1.1. Germanium

Due to its high refractive index and great dispersion characteristics, germanium is the most widely used lens material in the 8 to 12 μm (1250 - 833.3 cm^{-1}) region. The principal region of transparency extends from ≈ 1.8 to 18 μm (5555 - 555 cm^{-1}) at 300 K extending to ≈1.5 to 18 μm at 50 K. Due to this low dispersion property across a wide range of temperatures Ge is preferred in applications for which chromatic aberration is a problem. The various other properties like surface hardness, high mechanical strength, and good thermal conductivity make Ge an attractive material for IR applications. The short wavelength cut-off corresponds to an energy gap between 0.68 eV at 300 K to 0.83 eV at 50 K and a transmission level of approximately 47% from a refractive index of ≈ 4.0 [4]. Figure 1 shows the calculated transmission profile at 293 K for substrate thicknesses between 1.0 and 3.5 mm.

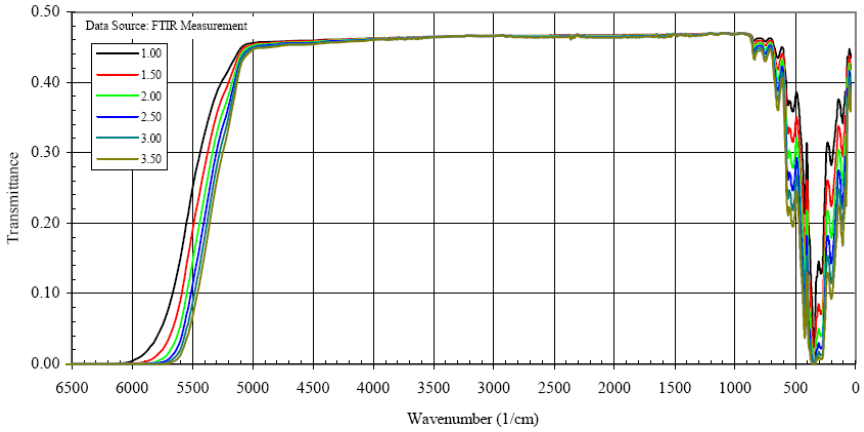

Figure 1. Calculated transmission profiles of germanium at 293 K in the range of 1.8-18 μm for substrate thicknesses between 1.0 and 3.5 mm [4].

Optical properties of germanium are quite sensitive to temperature difference. When the temperature increases above 100 °C its transmission profile degrades.

Germanium blocks ultraviolet, visible and infrared up to about 2 µm. Germanium has quite low absorption in the wavelength range of 8-12 µm range. Long wavelength absorption is caused by the phonon absorption. Figure 2 shows the wavelength dependent absorption coefficient.

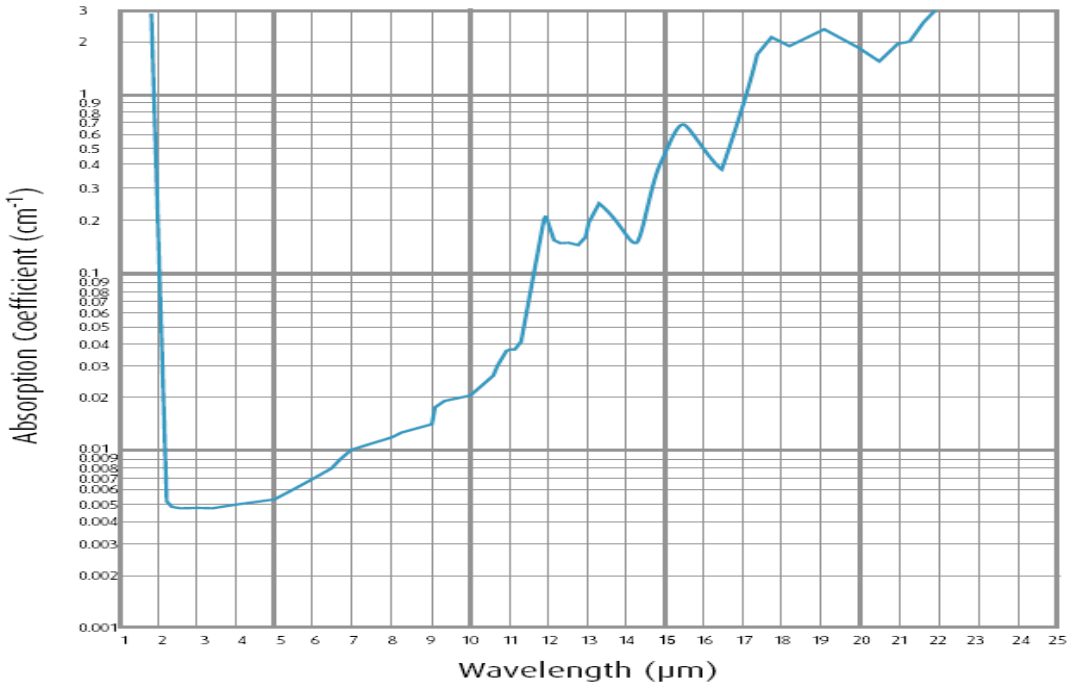

Figure 2. Absorption coefficient of germanium [5].

2.1.2. Zinc Selenide

ZnSe is another material widely used in thermal imaging systems to correct chromatic aberration caused by other refractive components in the system. It is transparent in the region 8-12 µm (20000 - 555 cm^{-1}). It is a soft, non-hygroscopic, and has a high resistance to thermal shocks. The bulk losses due to scattering and absorption are very low and that results in a superior optical transmission. All of these properties make ZnSe an ideal material

for optical elements in the IR region. The predicted substrate transmittance spectra of CVD ZnSe for substrate thicknesses between 2.0-4.5mm, is shown in Figure 3. At room temperature the electronic absorption edge is at 0.476 μm (21000 cm^{-1}) and far infrared multi-phonon absorption edge is at 22.2 μm (450 cm^{-1}) [4].

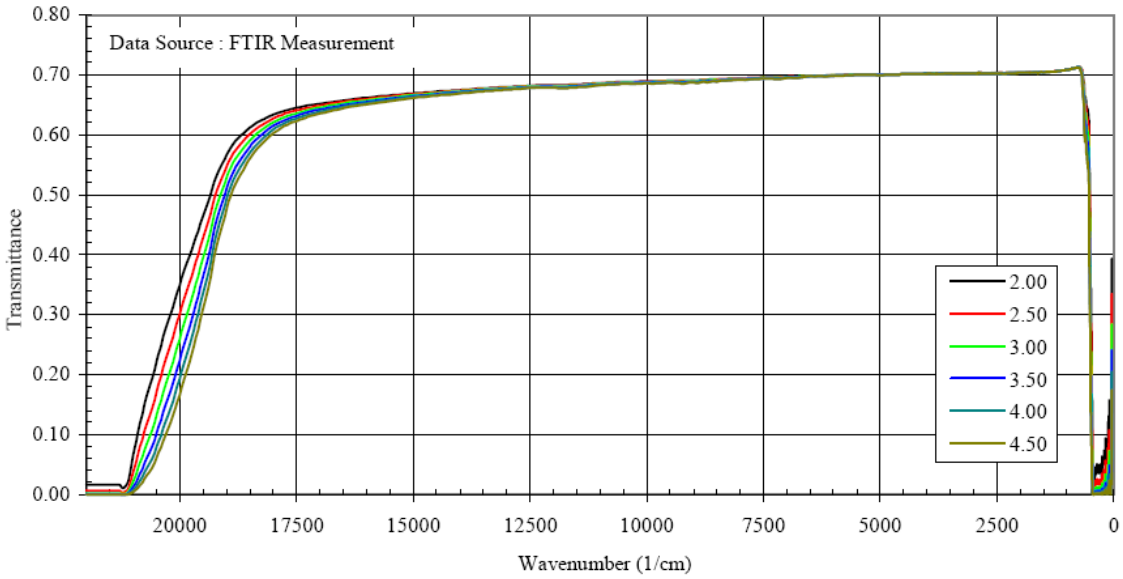

Figure 3. Calculated transmission profiles of zinc selenide at 293 K for thicknesses between 2.0 and 4.5 mm [4].

At room temperature in the visible and infrared range, the refractive index of ZnSe varies approximately from 2.66 (at 0.55 μm) to 2.33 (at 18 μm) as a decreasing function of wavelength and due to low extinction coefficient, transmission is high and uniform. The temperature dependence of the refractive index is not strong, for example at 12 μm it changes from 2.38 to 2.41 as the temperature increases from 90 to 630 K. For these reasons it is commonly used as a window material also in the production of optical elements.

2.1.3. Zinc Sulfide

ZnS is a wide gap semiconductor with direct band gap value of E_g =3.68 eV. It is commonly used as IR substrates since it has good mechanical strength and can be processed easily. Due to good transmission characteristics in the 3 to 12 μm (3333 - 833 cm^{-1}) region, it is suitable for thermal imaging systems. ZnS is used for anti reflecting coating purposes as well as for electro-luminescent device and solar cell applications. Furthermore, in CO_2 laser optics ZnS is the industry standard.

The transmittance of ZnS is shown in Figure 4 between 0.33 – 250 μm (30000 - 40 cm^{-1}) at room temperature for substrate thicknesses between 2-4.5 mm. The electronic absorption edge is at 0.33 μm (30000 cm^{-1}) and the multi phonon absorption is around 250 μm (40 cm^{-1}).

The refractive index of ZnS changes from 2.42 (at 0.50 μm) to 2.13 (at 18 μm) at room temperature. The refractive index at 12 μm in the temperature range of 90 – 630 K changes from 2.16 to 2.18, and varies very slight with temperature.

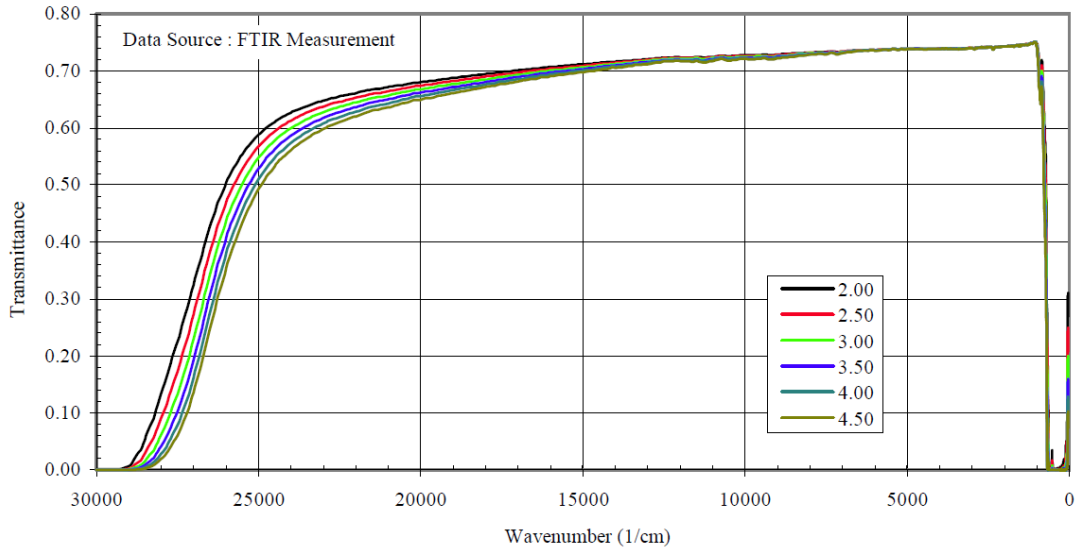

Figure 4. Calculated transmission profiles of zinc sulfur at 293 K for thicknesses between 2.0 and 4.5 mm [4].

2.1.4. Lead Telluride

Lead-telluride is a narrow-gap semiconductor with a direct energy of 0.32 eV, at room temperature. Various optical properties like persistent photo response enhanced responsive quantum efficiency and, radiation hardness of PbTe can be tailored by doping this material with group III impurities. Infrared detectors produced from PbTe are highly sensitive and very stable.

The refractive index of PbTe is one of the highest among the materials that are used in IR technology. In its thin film form, refractive index (n) varies in between 5.1 and 5.5 in the infrared region. Due to temperature variations the refractive index varies from 5.5 (at room temperature) to 5.85 (at 80 K). The transmittance of PbTe films grown at different substrate temperatures is shown in Figure 5.

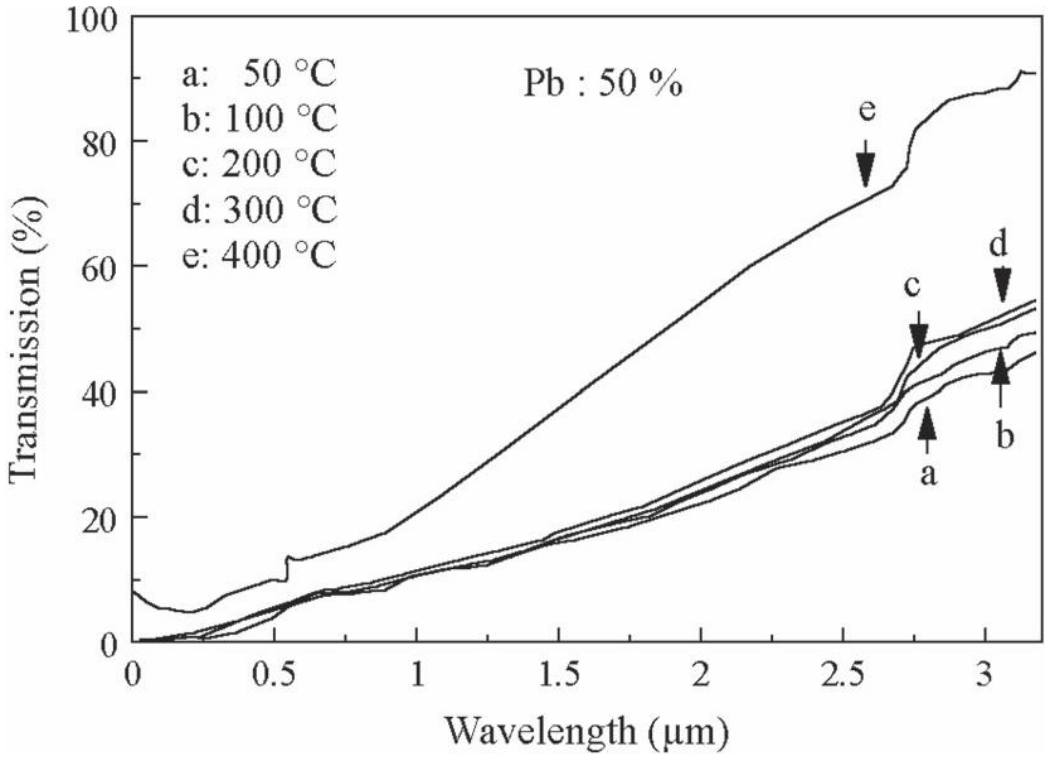

Figure 5. Transmission curves of films deposited from pellets with equal Pb and Te concentrations on substrates maintained at different temperatures [6].

The electronic absorption edge is at 3.5 μm at room temperature and this removes the need for the short wavelength blocking for the substrate material. Cooling moves this edge to longer wavelengths. This is due to high sensitivity of the band gap to temperature, at 77 K, E_g reduces to 0.22 eV. The corresponding wavelength shift is proportional to the inverse of temperature.

2.2. Fresnel Equations

As it is mentioned before the main idea behind designing an anti-reflection coating is to increase the fraction of energy transmitted through an optical element. In order to calculate that fraction of energy one should consider the electromagnetic wave nature of light. Fresnel Equations describe the behavior of light at an interface and also shows that, the fraction of energy transmitted through an interface, depends not only the refractive indices of the media but also polarization state of the incoming light. In this chapter, behavior of light at an interface and how polarization state of that light effect the energy transmitted through that interface will be investigated. For an electromagnetic wave at an interface it is convenient to start with a monochromatic plane wave described by;

$$\vec{E}_i = \vec{E}_{0i}\, e^{[i(\vec{k}_i . \vec{r} - w_i t)]} \tag{2.1}$$

$$\vec{E}_i = \vec{E}_{0i} \cos(\vec{k}_i . \vec{r} - w_i t) \tag{2.2}$$

Knowing that any polarization state of light can be described by two orthogonal linearly polarized waves, one free to choose the wave as linearly polarized which also means $\vec{E}_{0i}$ is constant in time.

Reflected and transmitted waves can also be expressed in the same form.

$$\vec{E}_r = \vec{E}_{0r} \cos(\vec{k}_r . \vec{r} - w_r t) \tag{2.3}$$

$$\vec{E}_t = \vec{E}_{0t}\cos(\vec{k}_t . \vec{r} - w_t t) \tag{2.4}$$

At the boundary, incident, reflected and transmitted waves exit simultaneously which means;

$$(\vec{k}_i . \vec{r} - w_i t) = (\vec{k}_r . \vec{r} - w_r t) = (\vec{k}_t . \vec{r} - w_t t) \tag{2.5}$$

And also at the boundary plane where $\vec{r} = 0$

$$w_i t = w_r t = w_t t \text{ or } w_i = w_r = w_t \tag{2.6}$$

In addition to the equality of frequencies, at t=0 within the boundary plane eqn. 2.6 gives

$$(\vec{k}_i \cdot \vec{r}) = (\vec{k}_r . \vec{r}) = (\vec{k}_t . \vec{r}) \tag{2.7}$$

First two term in the equation 2.7 gives

$$k_i r \sin\theta_i = k_r r \sin\theta_r \tag{2.8}$$

Incident and reflected waves propagate in the same medium. Thus, these two have the same wave number k meaning that incidence and reflection angles are equal. This is also known as "Law of Reflection".

$$\theta_i = \theta_r \tag{2.9}$$

The first and the third terms in eqn. 2.7 give the well known expression called "Snell's Law"

$$k_i r \sin\theta_i = k_t r \sin\theta_t \tag{2.10}$$

Substituting $k = \frac{n\omega}{c}$ Snell's law can be obtained as

$$n_i \sin\theta_i = n_t \sin\theta_t \tag{2.11}$$

As it is mentioned earlier in this chapter transmitted light intensity also depends on the polarization of the light. It is sufficient to examine two possible linear polarization modes of light since other types of polarizations can be explained as the linear combination these two. These modes are called transverse electric mode and transverse magnetic mode depending on the perpendicularity of $\vec{E}$ and $\vec{B}$ field to the plane of incidence, respectively.

A) Transverse Electric Mode (TE) If the $\vec{E}$ field is perpendicular to the plane of incidence, this is called transverse electric mode. One of the boundary condition of the laws of electromagnetism states that the tangential component of $\vec{E}$ and $\vec{B}$ field should be continuous across the boundary. This fact gives us

$$E_{0i} + E_{0r} = E_{0t} \tag{2.12}$$

$$B_{0i}\cos\theta_i - B_{0r}\cos\theta_r = B_{0t}\cos\theta_t \tag{2.13}$$

Electric and magnetic field amplitudes are related to each other with the equation;

$$E = \frac{c}{n}B \tag{2.14}$$

Then the equation 2.13 can be written as,

$$n_1 E_{0i}\cos\theta_i - n_1 E_{0r}\cos\theta_r = n_2 E_{0t}\cos\theta_t \tag{2.15}$$

Using equations 2.12 and 2.15 one can easily show that,

$$\frac{E_{0r}}{E_{0i}} = \frac{n_1\cos\theta_i - n_2\cos\theta_t}{n_1\cos\theta_i + n_2\cos\theta_t} = r_{TE} \tag{2.16}$$

r_{TE} is called "reflection coefficient" for TE mode. If eqns. 2.12 and 2.15 are solved for $\frac{E_{0t}}{E_{0i}}$, transmission coefficient t_{TE} for TE mode can be obtained as;

$$\frac{E_{0t}}{E_{0i}} = \frac{2n_1 \cos\theta_i}{n_1 \cos\theta_i + n_2 \cos\theta_t} = t_{TE} \tag{2.17}$$

B) Transverse Magnetic Mode (TM)

Like the $\vec{E}$ field, if the $\vec{B}$ field is perpendicular to the plane of incidence, this time it is called transverse magnetic field. Using the corresponding boundary conditions about the continuity of the parallel component of $\vec{E}$ and $\vec{B}$ field, it is quite straight forward to obtain the followings;

$$-B_{0i} + B_{0r} = -B_{0t} \tag{2.18}$$

$$E_{0i} \cos\theta_i + E_{0r} \cos\theta_r = E_{0t} \cos\theta_t \tag{2.19}$$

Recalling the equation 2.16 and solving these two equations for $\frac{E_{0r}}{E_{0i}}$ and $\frac{E_{0t}}{E_{0i}}$, gives reflectance and transmittance coefficients for TM mode, respectively. These coefficients are given in the equations 2.20 and 2.21.

$$\frac{E_{0r}}{E_{0i}} = \frac{n_2 \cos\theta_i - n_1 \cos\theta_t}{n_2 \cos\theta_i + n_1 \cos\theta_t} = r_{TM} \tag{2.20}$$

$$\frac{E_{0t}}{E_{0i}} = \frac{2n_1 \cos\theta_i}{n_1 \cos\theta_t + n_2 \cos\theta_i} = t_{TM} \tag{2.21}$$

Eqns. 2.16, 2.17, 2.20 and 2.21 are called Fresnel Equations. Using Snell's Law these equations can be written as;

$$r_{TE} = \frac{\sin(\theta_i - \theta_t)}{\sin(\theta_i + \theta_t)} \tag{2.22}$$

$$r_{TM} = \frac{\tan(\theta_i - \theta_t)}{\tan(\theta_i + \theta_t)} \tag{2.23}$$

$$t_{TE} = \frac{2\sin\theta_t \cos\theta_i}{\sin(\theta_i + \theta_t)} \tag{2.24}$$

$$t_{TM} = \frac{2\sin\theta_t \cos\theta_i}{\sin(\theta_i + \theta_t)\cos(\theta_i - \theta_t)} \tag{2.25}$$

Earlier in this chapter it is said that antireflection coatings are needed to maximize the transmitted power through an interface. "Reflectance" *R* and "Transmittance" *T* are the measures of the reflected and transmitted power, respectively. They are defined by;

$$R_{TE,TM} = \left(\frac{E_{0r}}{E_{0i}}\right)^2 = r^2{}_{TE,TM} \tag{2.26}$$

$$T_{TE,TM} = \left(\frac{E_{0t}}{E_{0i}}\right)^2 \frac{n_2 \cos\theta_t}{n_1 \cos\theta_i} = \left(\frac{n_2 \cos\theta_t}{n_1 \cos\theta_i}\right) t^2{}_{TE,TM} \tag{2.27}$$

For the lossless medium sum of the reflectance and the transmittance give the unity.

$$R_{TE} + T_{TE} = 1 \tag{2.28}$$

$$R_{TM} + T_{TM} = 1 \tag{2.29}$$

Another special case is the normal incidence, where $\theta_i = 0$. If this is the case, difference between two modes does not exist anymore and the equations 2.26 and 2.27 become;

$$R = R_{TE} = R_{TM} = \left(\frac{n_2 - n_1}{n_2 + n_1}\right)^2 \tag{2.30}$$

$$T = T_{TE} = T_{TM} = \frac{4n_1 n_2}{(n_1 + n_2)^2} \tag{2.31}$$

Another important point is the phase shift. From now, TE mode will be investigated for simplicity. Phase shift π occurs between incident and reflected light during the reflection if $\overrightarrow{E_{TE}}$ field reverses direction. That happens if incidence medium has lower refractive index than the emergent medium. At that point it is time to introduce the concept of interference. It is the superposition of two or more waves under very special conditions. These conditions are mainly the following; the waves should have the same frequency and need to be in phase. That is why phase shift is quite important.

Among many cases that result interference, interference in thin films is our concern. Some part of the incoming light is transmitted whereas the other part reflected back, when it hits the surface of a thin film. Transmitted part is also reflected back by the film to substrate interface as it is seen in the Figure 6. These multiple reflection goes on.

Let's consider the first two reflected beam. The second reflected beam travels $2t\cos\theta_t$ larger distance to reach the same point with the first reflected beam. This additional path times the refractive index of the medium is called "optical path difference" and can be denoted by Δ.

$$2n_t t\cos\theta_t = \Delta \tag{2.32}$$

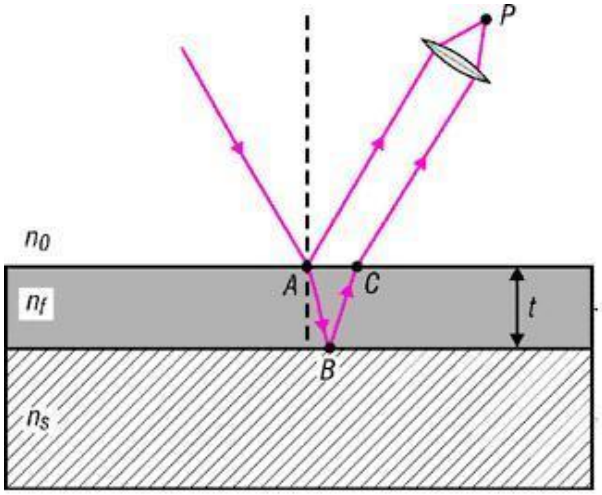

Figure 6. Two beam interference due to single thin film layer.

This optical path difference causes phase change. If $\Delta = \lambda$, the two beams are still in phase and there exist a constructive interference. However, as it is mentioned before, phase shift can also occur during reflection if the incident medium has lower refractive index. If this is the case an additional phase shift, π in other words $\lambda/2$ is also added to the phase. That makes the two beams out of phase, so the destructive interference occurs.

To simplify the explanation we have consider only two reflected beams. However, in reality these reflections are not limited by two, they go on and on. Such reflections are called multiple reflections.

Now it is necessary to define internal and external reflection concepts to make things easier. Shortly, if a light is reflected by a medium with higher refractive index than the incident medium, this is called "external reflection" whereas "the internal reflection" is the just opposite of external reflection.

In general r, t and r', t' are the abbreviation of the reflectance and transmittance coefficients at an external and internal reflections, respectively.

Let us call the amplitude of the incident beam; E_0 and angle of incidence; θ_i as it is seen in the Figure 7.

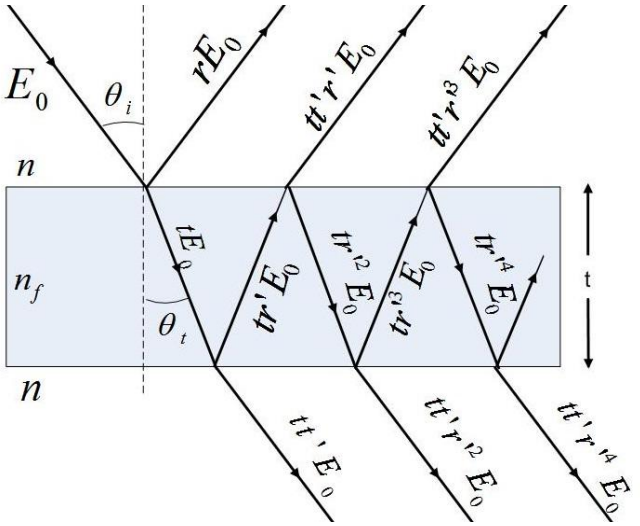

Figure 7. Multiple beam interference.

If the reflected beams are collected together with a lens they will form interference near normal incidence. This is called multiple beam interference. According to the Equation 2.32, phase shift between two successive reflected beams is

$$\phi = k\Delta \text{ , where } k = \frac{2\pi}{\lambda} \tag{2.33}$$

According to the Figure 7 first three reflected beams can be written as;

$$E_1 = rE_0 e^{i\omega t} \tag{2.34}$$

$$E_2 = tt'r'E_0 e^{i(\omega t-\phi)} \tag{2.35}$$

$$E_3 = tt'r'^3 E_0 e^{i(\omega t-2\phi)} \tag{2.36}$$

There are of course more reflected beams than three. In order to calculate total irradiance these waves should be superposed. Realizing that the Nth reflected wave can be written as

$$E_N = tt'r'^{2N-3} E_0 e^{i[\omega t-(N-1)\phi]} \tag{2.37}$$

Summation of the eqn. 2.27 over N gives the resultant reflected wave as

$$E_R = E_0 e^{i\omega t}[r + tt'r'e^{-i\phi}\sum_{N=2}^{\infty} r'^{(2N-4)}e^{-i(N-2)\phi}] \tag{2.38}$$

Using summation rules and simplifying the eqn. 2.38 becomes

$$E_R = E_0 e^{i\omega t}\left[\frac{r(1-e^{-i\phi})}{1-r^2e^{-i\phi}}\right] \tag{2.39}$$

Using the basic definition of irradiance; a time average of the delivered power per unit area, one can write

$$I = \varepsilon_0 c^2 < \left|\vec{E} \text{ x } \vec{B}\right| >= \frac{1}{2}\varepsilon_0 c E_R^2 \tag{2.40}$$

Then irradiances for reflected and transmitted waves can be found as;

$$I_R = \frac{2r^2(1-\cos\phi)}{1+r^4-2r^2\cos\phi} I_i \tag{2.41}$$

$$I_T = \frac{(1-r^2)^2}{1+r^4-2r^2\cos\phi} I_i \tag{2.42}$$

where $I_i = \frac{1}{2}\varepsilon_0 c E^2$ is the irradiance of the incident wave.

In most cases it would be useful to express the transmitted intensity, eqn. 2.42, in terms of the Airy function $A(\phi)$ as

$$I_T = \frac{tt'}{1-r^2} A(\phi) I_i \tag{2.43}$$

where $A(\phi) = \frac{1}{1+F\sin^2\frac{\phi}{2}}$ (2.44)

is known as the airy function. In this expression the coefficient of Finesse F is related to the reflectivity of the boundaries and defined by

$$F = \left(\frac{2r}{1-r^2} \right)^2 . \tag{2.45}$$

All these equations explain what happens to the light when it meets with a boundary. From that point of view, it is obvious that a multilayer film is a collection of interfaces. Calculating r and t for each layer and trying to find out the cumulative effect of all these layers is not practical. Instead, a mathematical method called "Matrix Method" will be more helpful to investigate the overall effect of a multilayer coating.

2.3. Matrix Method

Relationship between waves on both sides of a layer gives the characteristic matrix of that layer. This 2x2 matrix gives the reflectance and transmittance of the layer in addition to the optical parameters of that layer.

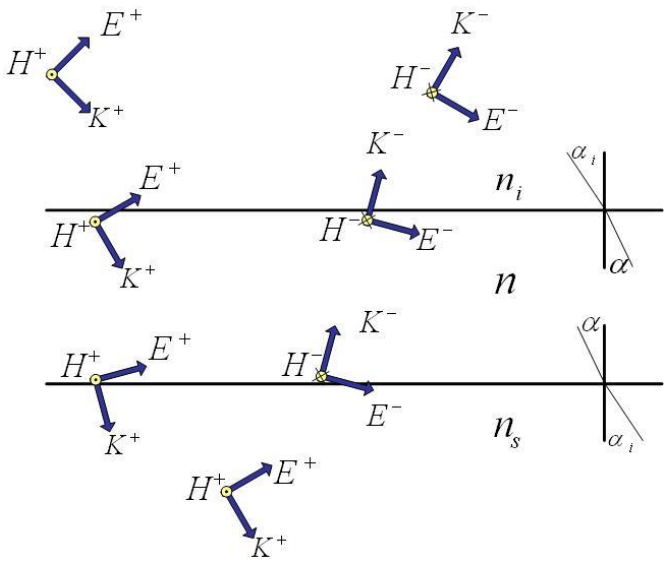

Figure 8. TE mode wave at an interface [7].

According to Figure 8, the boundary conditions about the continuity of the tangential component of the electric and magnetic field at boundary 1 give

$$E(x_1) = E^+(x_1 - \varepsilon) + E^-(x_1 - \varepsilon) = E^+(x_1 + \varepsilon) + E^-(x_1 + \varepsilon) \tag{2.46}$$

$$H(x_1) = \sqrt{\varepsilon_0/\mu_0}\left[E^+(x_1 - \varepsilon) - E^-(x_1 - \varepsilon)\right] n_i \cos\theta_i \tag{2.47}$$

$$= \sqrt{\varepsilon_0/\mu_0}\left[E^+(x_1 + \varepsilon) - E^-(x_1 + \varepsilon)\right] n \cos\theta_t$$

Where $E^+(x_1 - \varepsilon)$ and $E^+(x_1 + \varepsilon)$ represent the waves traveling in direction of incidence just above and below the boundary x_1, respectively. If the same equations are written for the waves at the second boundary,

$$E(x_2) = E^+(x_2 - \varepsilon) + E^-(x_2 - \varepsilon) = E^+(x_2 + \varepsilon) \tag{2.48}$$

$$H(x_2) = \sqrt{\varepsilon_0/\mu_0}\left[E^+(x_2 - \varepsilon) - E^-(x_2 - \varepsilon)\right] n \ \cos\theta_t \tag{2.49}$$

$$H(x_2) = \sqrt{\varepsilon_0/\mu_0}\left[E^+(x_2 + \varepsilon)\right] n_s \cos\theta_{t2}$$

are obtained. One should keep in mind that there is no reflected light in the exit medium so $E^-(x_2 + \varepsilon)$ terms in equations 2.48 and 2.49 are dropped. At that point there are two options. The first is to write E^+ and E^- terms at both boundaries, in terms of $E(x_1)$ and $E(x_2)$. This will lead to the characteristic matrix which includes only the optical parameters of the layer.

The second choice is to write $E(x_1)$ and $E(x_2)$ in terms of E^+ and E^-, instead. This will give a matrix with elements related to the transmittance and reflectance of the layer. This type of matrix is also called "The Transfer Matrix". Let us examine the first case.

According to the equations 2.32 and 2.33 a wave traverses the film once undergoes a phase

shift $\phi = k\Delta = \frac{2\pi}{\lambda} nt\cos\theta_t$ where t is the physical thickness of the film.

Then it is possible to connect the two waves at different boundaries as;

$$E^+(x_2 - \varepsilon) = E^+(x_1 + \varepsilon)e^{-i\phi} \tag{2.50}$$

$$E^-(x_2 - \varepsilon) = E^-(x_1 + \varepsilon)e^{+i\phi}$$

When we substitute the equation 2.50 in to 2.48 and 2.49 and solve these equations for $E^+(x_1 + \varepsilon)$ and $E^-(x_1 + \varepsilon)$, We will manage to write

$$E(x_1) = E(x_2)\cos\phi + \frac{\sqrt{\mu_0/\varepsilon_0}H(x_2)i\sin\phi}{n\cos\theta_t} \tag{2.51}$$

$$\sqrt{\mu_0/\varepsilon_0}H(x_1) = E(x_2)in\cos\theta_t\sin\phi + \sqrt{\mu_0/\varepsilon_0}H(x_2)\cos\phi \tag{2.52}$$

Defining the impedance of the free space $Z_0 = \sqrt{\frac{\mu_0}{\varepsilon_0}}$ turns equations 2.51 and 2.52 into

$$E(x_1) = E(x_2)\cos\phi + \frac{Z_0 H(x_2)i\sin\phi}{n\cos\theta_t} \tag{2.53}$$

$$H(x_1) = \frac{1}{Z_0}E(x_2)in\cos\theta_t\sin\phi + H(x_2)\cos\phi \tag{2.54}$$

If same calculations are carried on for the TM mode,

$$E(x_1) = E(x_2)\cos\phi + \frac{Z_0 H(x_2)i\sin\phi}{n/\cos\theta_t} \tag{2.55}$$

$$H(x_1) = \frac{1}{Z_0}E(x_2)i\frac{n}{\cos\theta_t}\sin\phi + H(x_2)\cos\phi \tag{2.56}$$

are obtained.

These two pairs of equations can be written in matrix form. For example, equations 2.53 and 2.54 give;

$$\begin{bmatrix} E(x_1) \\ H(x_1) \end{bmatrix} = \underbrace{\begin{bmatrix} \cos\phi & \frac{Z_0 i \sin\phi}{n\cos\theta_t} \\ \frac{1}{Z_0} in\cos\theta_t \sin\phi & \cos\phi \end{bmatrix}}_{M} \begin{bmatrix} E(x_2) \\ H(x_2) \end{bmatrix} \tag{2.57}$$

M is the characteristic matrix of a single layer. In general, if there are N layers, characteristic matrix of this system is the multiplication of the system matrices of the individual layer.

$$\begin{bmatrix} E(x_1) \\ H(x_1) \end{bmatrix} = M_1 M_2 M_3 ... M_N \begin{bmatrix} E(x_{N+1}) \\ H(x_{N+1}) \end{bmatrix} \tag{2.58}$$

$$M = M_1 M_2 M_3 ... M_N \tag{2.59}$$

As it is seen in the equation 2.57, M contains only the optical parameters of the thin film like refractive index and thickness.

In order to calculate reflectance and transmittance coefficients one should have to write $E(x_1)$ and $E(x_2)$ in terms of E^+ and E^-.This is the second case. Rewriting equation 2.57 using the equations 2.46, 2.47 and 2.49 let us to write;

$$\begin{bmatrix} E^+(x_1-\varepsilon)+E^-(x_1-\varepsilon) \\ \sqrt{\varepsilon_0/\mu_0}\left[E^+(x_1-\varepsilon)-E^-(x_1-\varepsilon)\right] n_i\cos\theta_i \end{bmatrix} = M_1 \begin{bmatrix} E^+(x_2+\varepsilon) \\ \sqrt{\varepsilon_0/\mu_0}\left[E^+(x_2+\varepsilon)\right] n_s\cos\theta_{t2} \end{bmatrix} \tag{2.60}$$

Keeping in mind that the each wave is the sum of the all waves traveling in that direction we can write

$$r = \frac{E^-(x_1-\varepsilon)}{E^+(x_1-\varepsilon)} \quad \text{and} \quad t = \frac{E^+(x_2+\varepsilon)}{E^+(x_1-\varepsilon)} \tag{2.61}$$

Then the eqn. 2.60 can be written as

$$\begin{bmatrix} 1+r \\ \sqrt{\varepsilon_0/\mu_0}\left[1-r\right]n_i\cos\theta_i \end{bmatrix} = M_1 \begin{bmatrix} t \\ \sqrt{\varepsilon_0/\mu_0}tn_s\cos\theta_{t2} \end{bmatrix} \tag{2.62}$$

When the matrices are expanded, eqn. 2.62 gives the reflectance and transmittance amplitudes in terms of the characteristic matrix elements. The following equations give these relations;

$$r = \frac{\kappa_0 m_{11} + \kappa_0\kappa_s m_{12} - m_{21} - \kappa_s m_{22}}{\kappa_0 m_{11} + \kappa_0\kappa_s m_{12} + m_{21} + \kappa_s m_{22}} \tag{2.63}$$

$$t = \frac{2\kappa_0}{\kappa_0 m_{11} + \kappa_0\kappa_s m_{12} + m_{21} + \kappa_s m_{22}} \tag{2.64}$$

Where we define, $\kappa_0 = \sqrt{\varepsilon_0/\mu_0}\,n_i\cos\theta_i$ and $\kappa_s = \sqrt{\varepsilon_0/\mu_0}\,n_s\cos\theta_{t2}$ for simplicity.

2.4. Anti-Reflection Coating

Antireflection coatings are quite necessary in thermal imaging systems due to the high refractive index materials used in such systems. These coatings are designed to reduce reflections caused by the sharp refractive index changes at the material to air interface. In addition to the intensity loss, stray light is another result of reflections which reduces the image contrast, therefore image quality.

The most primitive form of the antireflection coating consists of a single quarter wave layer. However, such a coating only eliminates reflections at one wavelength. Using the characteristics matrix for a single film it is easy to write

$$T = \frac{4}{2 + n_i/n_s + n_s/n_i + \left(n_s - n^2/n_s\right)\left(n_i/n^2 - 1/n_i\right)\sin^2\Delta}. \tag{2.65}$$

For $\Delta = 0, \pi, 2\pi, ...$ and $n_i < n < n_s$ $\sin^2\Delta$=0 and T reaches its minimum value.

$$T_{\min} = \frac{4n_i n_s}{\left(n_i + n_s\right)^2} \tag{2.66}$$

Using $T+R=1$, $R_{\min}$ found as;

$$R_{\max}=\frac{(n_s-n_i)^2}{(n_s+n_i)^2}. \tag{2.67}$$

This equation is the same equation as equation 2.30. In other words, maximum reflectance of a single layer is equal to the reflectance of an uncoated substrate.

Another extremum of the equation 2.65 occurs at $\Delta=\pi/2,3\pi/2,....$ and for these values of Δ transmittance reaches its maximum value as;

$$T_{\max}=\frac{4n^2n_in_s}{\left(n_in_s+n^2\right)^2} \tag{2.68}$$

where

$$R_{\min}=\frac{(n_in_s-n^2)^2}{(n_in_s+n^2)^2} \tag{2.69}$$

Equations 2.68 and 2.69 are the equations what we are looking for. Eqn. 2.69 gives the refractive index of the layer material in addition to the optical thickness of the layer as

$$n=\sqrt{n_in_s} \quad \text{Where, } nd=\lambda/4,3\lambda/4..... \tag{2.70}$$

In that case, $R_{\min}=0$.

If similar calculations are carried on refractive index equation and the optical thicknesses of a two layer anti- reflection coating can be found as [7]

$$\frac{n_1}{n_2}=\sqrt{n_s/n_i} \text{ where, } nd=\lambda/4,3\lambda/4..... \tag{2.71}$$

2.5. Design of a Multilayer System

There are two aspects when designing a multilayer coating. The first is to refine an existing design with respect to the spectral response required and the second one is to synthesis a coating with the help of mathematical tools.

Although refining an existing design has its own advantages like achieving the desired spectral response quickly, this achievement highly depends on the starting design. Thus, it has great importance to choose an appropriate starting design. However, usually it is hard or impossible to find a good starting design. On the other hand, synthesis methods do not require an existing starting design. Because they construct their own starting design optimize it. For both methods to test the validity and the success of optimization, one needs a numerical measure of consistency with desired performance. This is commonly done by using the merit function which is a single valued function defined by the various required parameters of the system. Some of these parameters are transmittance T (or reflectance R) at a given wavelength, plane of polarization and the angle of incident [8].

Since the performance of the design is mainly determined by the interference effects of the waves multiply reflected from the various layer of the system the most important physical parameters would be the phases and the amplitudes of these waves. In the theory part of this thesis it has been shown that the phases and the amplitudes of these waves depends on the layer thickness and their indices of refraction. Choosing the thickness or the refractive index as the optimization parameter one arrives at a minimized merit function which cannot further be minimized by the variation of these parameters. In recent years the most prominent method of multilayer coating optimization technique, named as needle optimization method, is discussed by Tikhonravov and Trubetskov [9]. In literature the basic idea of this technique was first proposed by Tikhonravov [10] in 1982.

According to the needle method new layers are inserted to the multilayer system. Each new layer gives a new parameter to the designer to re-optimize the design. This insertion continues until the design reaches the desired performance.

At that point there arise two questions: What should be the starting design? And where should be the needle layer inserted? The answer to the first question comes from Baumeister [11]. A Multilayer; composed of many thin layers, one or a few thick layers and combinations of these two are the three possible starting design structures. The answer to the latter question depends on the merit function. The best place is where the merit function

reaches a smaller number after the insertion of a needle layer. In recent years all these calculations are carried out by some commercially available thin film design software. In this work one of those programs called “The Essential Macleod” is used.

2.6. Thin Film Deposition Techniques and Thickness Control

Thin film deposition processes can be divided into parts: Physical Vapor Deposition (PVD) and Chemical Vapor Deposition (CVD). In PVD processes, source materials that are to be coated on the substrate are solid, whereas, in CVD, source materials are liquids or gases. Also reaction mechanism is different between these two techniques. In PVD, momentum transfer between the source atoms and evaporation of source atoms are the main mechanisms of deposition (expect from the reactive PVD processes). However, in CVD purely chemical reactions occur during the deposition. Generally, PVD is used for depositing metals, alloys and compound materials. On the other hand, CVD is mainly used for depositing dielectric thin films (except from Tungsten) and semiconductor thin films. Also these two techniques can be compared by means of some deposition parameters such as step coverage and deposition rate. Generally, PVD has much higher deposition rate than the CVD. On the contrary, CVD has better step coverage than the PVD since it uses gases as precursor [12]. Lastly, throughput (amount of substrate that is deposited in one process) is better in CVD systems.

In all deposition methods the control of the thickness of the films to be grown plays a crucial role in the performance of the final device. The most commonly used thickness measuring systems are the optical monitoring and the quartz crystal monitoring.

2.6.1. Physical Vapor Deposition

By using PVD systems large variety of materials such as metals, semiconductors, alloys and compounds can be easily deposited. They have wide range of applications in microelectronics industry such as creating metal or alloy interconnection layers and in optics to create compound and semiconductor antireflection coatings for optical components. A wide range of thicknesses can be achieved ranging from angstroms to millimeters, since high deposition rates can be obtained (up to 25 μm/sec) by PVD systems [12]. PVD processes mainly divide into two categories as evaporation and sputtering. They are different from each other in the aspects of how the source material is transferred into the vapor phase. There

is also one another technique called ion-planting process which is hybrid process containing fundamentals of evaporation and sputtering process. In this work, only evaporation and sputtering techniques will be discussed.

2.6.1.1. Evaporation

The purpose of this process is to vaporize or sublimate source material which is located at a certain distance from the substrate in order to create a film growth. The system contains an evaporation source to sublimate or vaporize the target material, a heater to control the temperature of substrate if desired. The evaporation process is performed in low pressure ranging from 10^{-5}–10^{-10} Torr. Low pressures are necessary since the melting point of materials decreases as pressure decreases. In addition, in this pressure range, the evaporated atoms go through a collisionless path before condensation on the substrate, thus film formation occurs directly above the source material. The growth rate decreases as distance between source and substrate increased. Generally, to increase thickness uniformity which is very important both in optical coatings and microelectronics, the planetary circular substrate holders which can also rotate are used.

Evaporation method can be divided into several groups in terms of the ways that evaporates the source material. Some these methods are resistance, arc, induction, electron beam and laser evaporators. Most commonly used ones are resistance heated (A) and electron beam evaporators (B) which will be discussed in this work.

A) Resistance Heated (Thermal) Evaporation

This evaporation technique relies on joule heating of metal filaments. The simplest thermal evaporator heaters are resistance heated wires and metal foils. Obviously, such heaters must provide the temperature that necessary to evaporate the source material and must have a negligible vapor pressure when compared to source material [13]. Moreover, at evaporation temperatures these heaters must not create contamination, undergo reaction with the source material or make alloys with the source material. Most commonly used heater materials are tungsten, molybdenum and tantalum which have very high melting points. Generally, these heaters are in the shape of dimpled strip and boat to hold enough amounts source materials. Upon melting, liquid form of source material covers the filament and held there by surface tension. This increases the evaporation surface area and thermal contact. Generally, the

necessary current that flows through to filament of evaporator is in the range of 20 to 500 amps to evaporate the source material [12].

The disadvantages of thermal evaporation systems are contamination by the filament boats and limitations of low input power levels. Therefore it is difficult to deposit pure thin films and evaporate materials that have high melting points [13].

B) Electron Beam Evaporation

In this technique, target material atoms are evaporated by using an electron gun source at low pressures. Electron beam (e-beam) evaporation technique has two major advantages over the thermal evaporation; one is that it has higher input power density and the other is that source material is loaded into a water-cooled crucible which is generally copper, therefore it eliminates the possible crucible contamination [12]. As a result of this melting point of the source material is not important for e-beam evaporation and good deposition rates can be achieved unlike thermal evaporation.

In the general setup of an e-beam evaporator, electrons are thermionically fired from a heated filament. These filaments are shielded from the line of sight of evaporation source and substrate thus eliminating the contamination of heated filament. Electrons are accelerated by grounded anode and negatively biased cathode. Moreover, in order to deflect electrons to the source material that is also grounded transverse magnetic is applied. In thermionic e-guns, there is limitation for the deposition around 1mTorr. Higher pressures causes more electron scattering and decreases cathode life time

The curling of the electron beam and non uniform beam density are the two main problems on the e-beam evaporation sources. In theory, electron beam should collide to source material at normal incidence. However, if magnetic field is somehow misaligned, electron beam may collide to source material with some angle, resulting in a shift in the growth rate of the thin film thus variable film thickness occurs. In order to overcome with this problem, focal spot size of the e-beam can be change and focused electron beam can be swept over the source material.

2.6.1.2. Sputtering

The sputtering process can be defined as ejection of particles from a solid surface due to impact of energetic particles to that surface. It is a statistical process that results from momentum transfer between energetic particles such as ions, neutral atoms and electrons that initiate cascade collisions on the target surface.

In sputtering deposition, source of coating material, namely target material, and substrate are placed face to face in a vacuum chamber which can be evacuated to pressure range of 10^{-5} to 10^{-7} Torr [12]. In order to provide collision of charged particles, target is negatively biased and substrate is connected to ground. Inert gases such as Ar are used to create glow discharge plasma in the vacuum environment and thus generate ions that bombard the target material. Generally, process pressures are in the range of 1 to 100 mTorr [14]. Figure 9 shows basic configuration for a sputtering system.

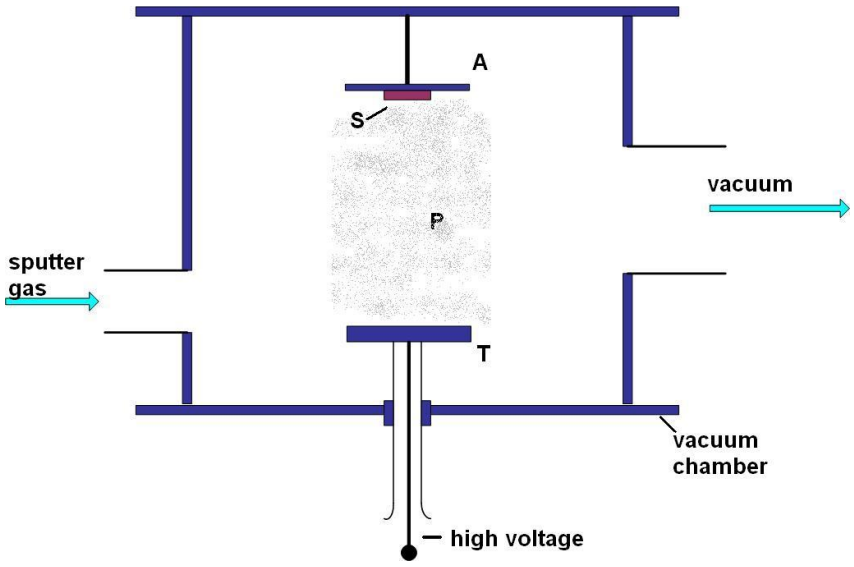

Figure 9. Basic configuration of a sputtering system. S indicates substrate, T indicates target, A indicates anode and P is plasma [15].

The ion-surface interactions have an important role for characterization of growing thin film and modifying their properties. After generating glow discharge and thus producing Ar ions several interactions occur on the target surface.

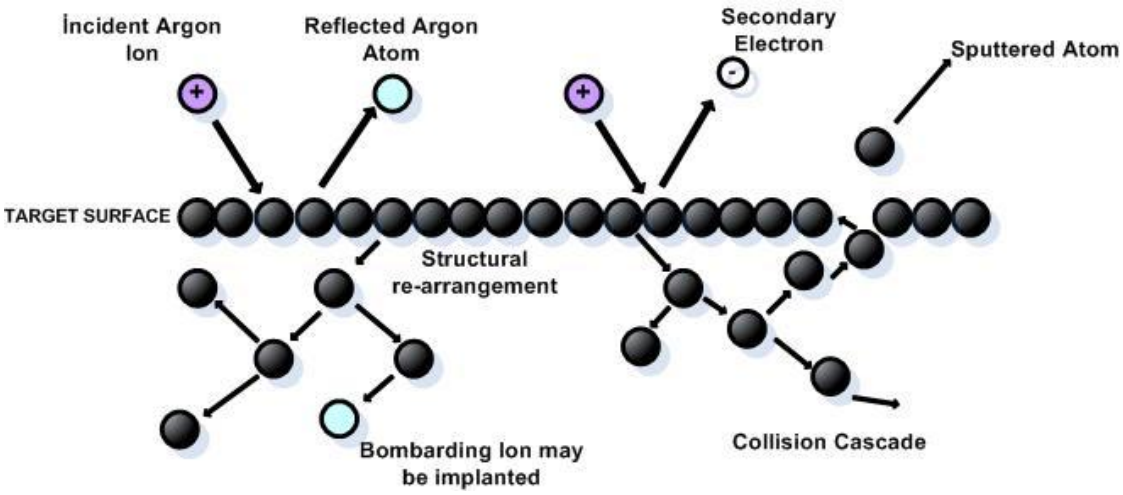

Figure 10. Interaction between Ar ions and surface of target material during sputtering [16].

The following interactions take place during ion bombardment as show in Figure 10:

- Firstly, ion may be reflected back from the surface of the target material. The reflection probability increases if the incident ion has lower mass than the target atom. Therefore it is important to use heavy inert gases such as Ar when creating glow discharge plasma.
- Secondly, ion may be implanted to target.
- The ion-surface interactions may cause structural changes on the surface of the target such as defects and vacancies. Moreover, it may also cause stoichiometric changes on target. These modifications on the target affect the structure of the deposited film.
- Secondary electrons might be created due to ion-surface interactions. If a correct sputtering configuration is used, these electrons collides inert gas atoms in the vacuum and increases the number of the bombarding ions. This helps to increase deposition rate.
- Finally, the ion impact to the target results in cascade collision on the surface of the target leading to ejection of target atoms. These atoms form a thin film on the

surface of the substrate.

Sputtering deposition is very versatile process due to its universality. In theory, any material may be sputtered, since target material is transformed into vapor phase via momentum transfer instead of chemical or thermal process. Moreover, sputter deposition has many variations to form thin film materials such as:

- Compound materials from a single target
- Alloys by using several targets
- In-situ layered coatings by using several targets sequentially

Moreover, the properties of deposited thin films can be changed by introducing a reactive gas into the vacuum chamber and electrically biasing the substrate to create ion bombardment on the growing film during the deposition.

As mentioned before, the ability of deposition of huge range of materials from elements to allays and compounds without changing their compositions make sputtering process applicable vast range areas such as optics, microelectronics, IC, automotive industry. In optics, it used for increasing or decreasing the transmission of optical components, creating filters or mirrors. In electronics industry, sputtering system have very important role in the fabrication of transducer and integrated circuits. In automotive sector, it is mainly used for metalizing plastic automotive parts [14].

There is wide range of sputtering system types used nowadays. The reasons for the requirement of different configuration may be listed as:

- To increase sputtering rate by increasing ion supply
- To increase available deposition area by increasing target size to deposit larger substrates
- To reduce the effects of temperature on the target material due to plasma heating
- To reduce process pressures to increase uniformity of the coated material

The sputtering systems may be divided into four categories as DC-diode, RF diode, Magnetron and Reactive sputtering. Only magnetron sputtering will be discussed since it is used in this work.

Magnetron Sputtering:

In magnetron sputtering systems, plasma is confined by a magnetic field that is provided by magnetrons placed behind the target. This kind of systems can be taught as a diode sputtering system supported with a magnetic field. However, magnetic field increases ionization efficiency near the target. In diode sputtering systems, the probability of collision of ions to the chamber walls is large. Moreover, ionization efficiency is reduced since the number of primary electrons hitting the anode without experiencing collisions is increased when the pressure is decreased. As a result there is a limitation on the process pressure and ionization efficiency is low for diode type sputtering. On contrast, magnetron sputtering systems overcomes these problems.

In magnetron sputtering systems, the magnetic field that is produced by magnetrons are parallel to the surface of target where they form electron traps and restricts the path of primary electron motion near the target surface. The trapped motion of electrons decreases probability of hitting walls of chamber walls and increases probability of collisions with gas atoms resulting in newly produced ions. Due to this high efficiency process, the working pressure can be lowered to 1mTorr and provides higher deposition rates [12]. Moreover, heating of substrate is reduced greatly since the probability of colliding electrons to the substrate is reduced greatly. This provides deposition of heat sensitive substrates.

DC and RF power can be used the produce glow discharge plasma for magnetron sputtering systems. The RF sputtering is required to deposit dielectric films which cannot be sputtered by the DC methods. The reason for that is the charge accumulation on the dielectric target surface due to DC power.

2.6.2. Chemical Vapor Deposition

In a CVD process, the gas phase precursors are transferred to a reaction chamber where the substrate is placed. Then, the precursors are activated thermally or by plasma in order to create a reaction at the surface of substrate to form a thin film. Materials with different properties can be obtained by changing process condition such as temperature or plasma power, gas flows and total gas pressure.

CVD has many applications in thin film industry. For example, it is used to deposit dielectric

layers, passivation layers, oxide barriers etc. in microelectronics industry. The production of optical fibers and heat resistant layers are possible with this technique. In addition, CVD is widely used in solar cell industry. Another reason of the usage of CVD so widely is its ability of depositing dielectrics, semiconductor compounds, organic and inorganic compounds either crystalline or amorphous form as desired. Moreover, stoichiometry of the deposited thin films can be controlled easily. **A**morphous silicon, poly-silicon, various silicon oxide films (low temperature oxide, high temperature oxide), borophosphosilicate glass (BPSG), tungsten and silicon nitride are the most common materials that can be deposited by CVD.

There are several types of CVD processes. Most commonly used types are atmospheric pressure (APCVD), low pressure (LPCVD) and plasma-enhanced (PECVD). In addition to these systems, there exists metal-organic CVD (MOCVD) and laser-enhanced (LECVD) systems which will not be discussed in this work.

2.6.2.1. Atmospheric Pressure Chemical Vapor Deposition

In APCVD systems, gaseous precursors are activated thermally at atmospheric pressure and resulting reaction forms thin film at the surface of substrate. APCVD processes are used for depositing high quality epitaxial thin films. In order to obtain such films, high temperatures (900°C-1200°C) are often required.

There are two main types of reactors used in APCVD systems; hot wall and cold wall reactors. Hot wall reactors use quartz tubes surrounded by heaters. Advantage of hot wall reactors is coating large number of substrates. However, at the walls of quartz tube deposition occurs and this causes contamination at the reaction chamber. Hot wall reactors are suitable for exothermic reactions since high temperature prevents deposition on the quartz tube walls. On cold wall reactors, only the substrate holders are heated by RF inductors or radiation lamps. As a result of this, contamination of the walls of the tubes is reduced. These types of reactors are ideal for endothermic reactions.

2.6.2.2. Low Pressure Chemical Vapor Deposition

LPCVD systems are similar to APCVD system except from that they use vacuum system in order to provide low deposition pressures such as 100 mTorr. Lower pressures provide more

surface kinetics control, good deposition uniformity and good step coverage. Another advantage of LPCVD over APCVD is that, it is possible to deposit more substrate in one batch since substrates can be installed more densely due to larger mean free path of gaseous at lower pressure. Most commonly, silicon nitride, polycrystalline Si and silicon dioxide thin films are deposited by using LPCVD systems.

2.6.2.3. Plasma-Enhanced Chemical Vapor Deposition.

In PECVD systems, the gas phase chemical reactions are produced by using glow discharge plasma and as a result thin film deposition occurs at the surface of substrate. In this technique, gas molecules are separated by impact of electrons, thus reactive neutral and ion particles are generated. These particles react with each other at the surface of the substrate resulting in thin film deposition. The glow discharge plasma during the process is generally activated by an RF field at low pressures. The reason of using RF sources is that most of the thin films deposited by PECVD are dielectrics and DC sources are not suitable for dielectric films. As mentioned, gas molecules are activated by the plasma instead of thermal energy, the reaction temperature drops drastically. The coatings can be obtained with technique generally at 300°C [12]. This property of PECVD makes it a very valuable system among the IC industry, since silicon-nitride films are used for passivation and encapsulation at the final stages of IC production and at this stages chips cannot be heated much above 300°C [13]. Although deposition temperature is low for PECVD process, the temperature parameter still has an active role on the quality and properties of the deposited films. Since, the diffusion and mobility of the absorbed radicals on the surface of the substrate are affected by the substrate temperature. Higher substrate temperature provides denser films and lesser hydrogen content. Moreover, substrate temperature has effects on the stoichiometry of the film.

2.6.3 Thickness Control

Thin film thickness monitoring instruments are used to measure thickness and deposition rate of the deposited film during the deposition at high vacuum. There are several ways to measure the film thickness during deposition. As long as a parameter that changes with the thickness is found, this parameter can be correlated to the thickness. There are several parameters that can be correlated to the thickness such as mass, electrical resistance, optical density, reflectance and transmittance. Among these most commonly used ones are optical

measurements of reflectance or transmission and measurements of deposited mass by quartz-crystals [17].

Since it is not possible to place thickness monitors as same place with the substrate, deposition thickness will be different for thickness monitor sensor and substrate. The ratio of the two is called tooling factor. The tooling factor can be calculated by measuring real thickness of the deposited film on the substrate and comparing it to the measured value on the thickness monitor.

Optical monitoring systems use a light source to illuminates the substrate that is to be measured and by using a detector reflected light from the surface of the substrate is measured. In this work quartz-crystal monitoring instrument was used and will be discussed in detail.

2.6.3.1. Quartz-Crystal Monitor

The mechanical vibration of a quartz crystal can be converted into electric signals due to piezoelectric properties of quartz. Any change of the quartz' mechanical property will result in shift on its resonant frequency. The change of mechanical property of quartz may be result from change in temperature or mass. If a quartz crystal monitoring system is exposed to a deposition, the resonance frequency of quartz changes due to change in the total mass of the crystal because of deposition. Then this change in the frequency is converted into a measure of film thickness by using the material constants such as z-ratio and density of the deposited thin-film.

There are two main problems with the quartz monitoring system. First one is that, as the deposition builds up of mass the accuracy of crystal is decreased. The crystal must be cleaned or changed with a new one. Secondly, for some applications, temperature of the crystal must below 120 ^{o}C to decrease effects of temperature coefficient. Therefore, it may not be possible to keep crystal and substrate at the same temperature [17].

CHAPTER 3

EXPERIMENTAL

3.1. Material Selection

Although there is large number of materials in the visible region, in the infrared part of the spectrum this numerous choice of materials is drastically reduced. Among these limited number of materials, germanium, zinc selenide and zinc sulfide were chosen as substrate materials. Lead telluride and zinc selenide were selected to be high and low index layer materials, respectively.

3.1.1. Substrate Characterization

3.1.1.1. Ellipsometry

An ellipsometer measures the change in the polarization state of the light, more specifically s and p component of the $\vec{E}$ field upon reflection and it uses this information to calculate material's complex refractive index or dielectric function. The basic ellipsometry set up can be seen in the Figure 11.

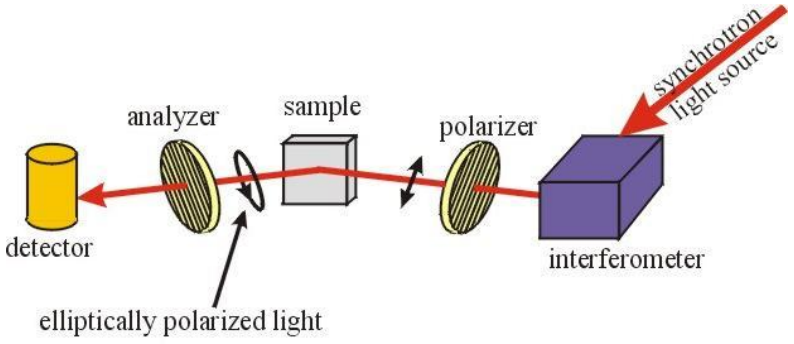

Figure 11. Typical ellipsometer set up [18].

It consists of a light source, two polarizers and a detector. The light coming from the source is linearly polarized by the first polarizer. Then it hits and is reflected by the sample. During this reflection s and p polarized parts of the $\vec{E}$ field experiences different phase shifts so the light becomes elliptically polarized. Then, the ellipse of the light is measure by the second polarizer that is why it is called analyzer.

The parameters that an ellipsometer measures directly are Ψ and Δ. These are amplitude ratio and the phase difference between p and s polarized light waves. The equation relating the reflected p and s polarized light amplitudes and the (Ψ , Δ) is given as;

$$\rho = \tan\psi e^{i\Delta} = \frac{r_p}{r_s} \tag{3.1}$$

By using the definition of the reflectance amplitude coefficient, r, one can say that Ψ represents the angle determined from the amplitude ratio between reflected p and s polarizations, while Δ express the phase difference between reflected p and s polarizations [19]. However, determination of these parameters is not enough to end the measurement. Another important part of an ellipsometric measurement is the data analysis. Data analysis includes determination of the dielectric functions and fitting this function to a dielectric function model. These models are Drude, Sellmeir, Cauchy, Lorentz and some combinations of these individual models. Which model is to be chosen depends on the region of transparency. For example in the transparent region Sellmeir is widely used whereas Drude model is preferred where absorption exists.

Since in the modern ellipsometers data acquisition and analysis are carried on by the commercially available softwares theoretical consideration are not discussed in details in this work.

3.1.1.2. Fourier Transform Infrared Spectroscopy

Infrared (IR) spectroscopy is a chemical analytical technique, that measures the intensity as a function of wavelength (or wave number) of infrared light. The dispersive type early IR instruments scan slowly because they use a prism or a grating. FT-IR stands for Fourier Transform Infra Red and was developed to overcome the limitations of the dispersive method. FTIR has the major advantages like speed, sensitivity, mechanical simplicity. In

infrared spectroscopy, IR radiation sent to a sample is partially absorbed by the sample and partially transmitted. The resulting irradiance versus wavelength characteristics represents the molecular absorption and transmission and hence the molecular fingerprint of the sample. Since no two unique molecular structures produce the same infrared spectrum infrared spectroscopy is very useful for many different of investigations.

A Fourier Transform Infrared (FTIR) spectrometer obtains infrared spectra by first collecting an interferogram of a sample signal with an interferometer, which measures all of infrared frequencies simultaneously. An FTIR spectrometer acquires and digitizes the interferogram, performs the FT function, and outputs the spectrum.

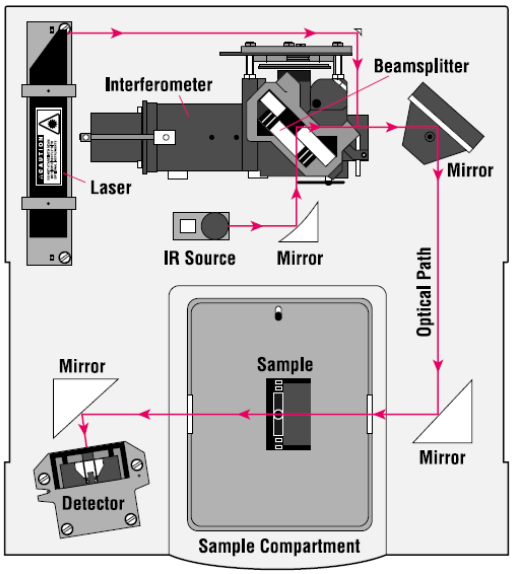

Figure 12. Schematic diagram of a FTIR [20].

In an interferometer (see Figure 12) incoming infrared beam is divided into two optical beams by a beam splitter. One beam reflects off of a fixed plane mirror. The second beam reflects off of a flat mirror which travels a very short distance away from the beam splitter. The two reflected beams are recombined when they meet together at the beam splitter and interfere. This signal is called interferogram and it has every infrared frequency “encoded” into it. When the interferogram signal is transmitted through or reflected off of the sample

surface, the specific frequencies of energy are adsorbed by the sample. The signal after interaction with the sample becomes the characteristic of the sample. The final beam arriving at the detector is measured. The detected interferogram needs to be "decoded" in terms of Fourier Transformation. The computer performs the Fourier transformation calculation and presents an infrared spectrum as the adsorbance (or transmittance) versus wave number.

A single beam spectrum generated by the Fourier transformed interferogram is a plot of raw detector response versus wave number. A background spectrum due to instrument and the environments should always be taken to normalize the FTIR measurement. Therefore the result of the transmittance spectrum is expressed as the ratio the irradiance transmitted by the sample to that due to background.

3.1.2. Measurement Results

Optical properties of substrate materials have investigated by FTIR spectrophotometer and ellipsometer. Bruker FTIR spectrophotometer was used in this work to obtain transmission spectra of the substrate materials. In Figures 13 to 18 measured transmission and reflection profiles of 3 mm thick Ge, ZnS and ZnSe substrates at 300 K are given.

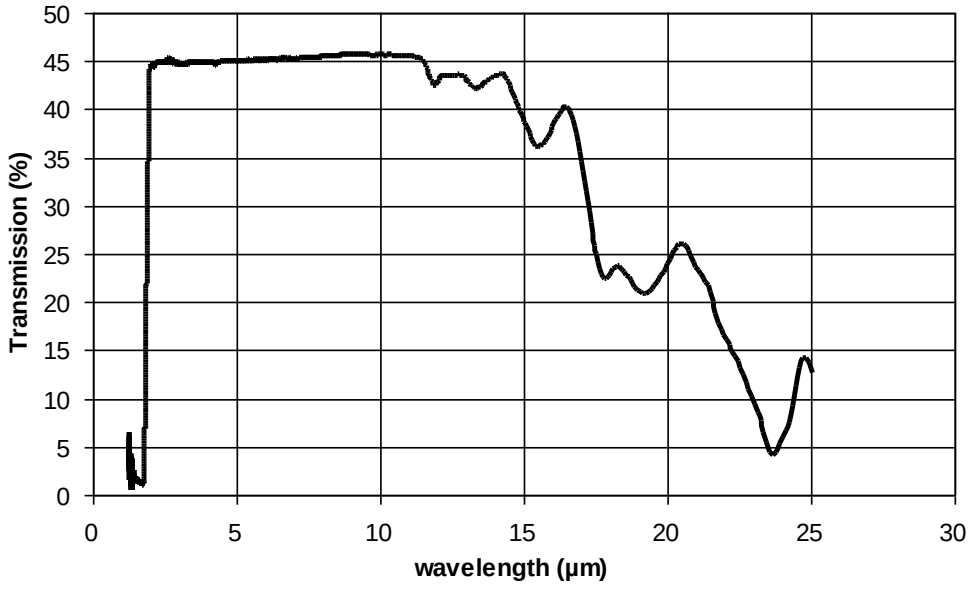

Figure 13. Measured transmission of 3 mm thick Ge at 300 K.

Almost 60 % of the incoming radiation is reflected because of the great refractive index difference between air and Ge interface. In Figure 14 reflection vs. wavelength is given for 3 mm thick double-sided polished Ge substrate at 300 K.

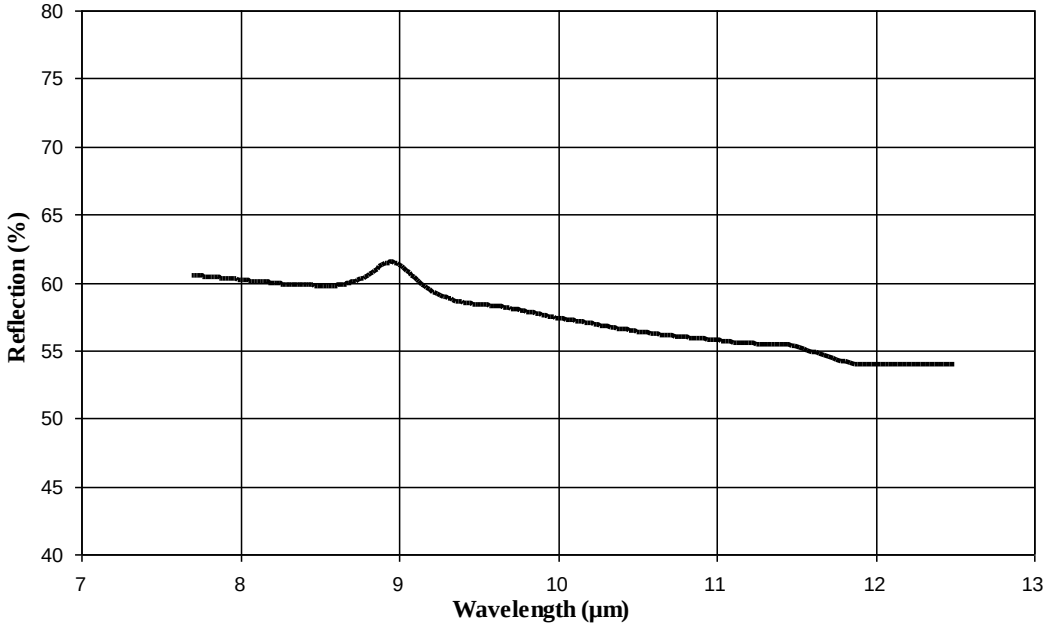

Figure 14. Reflection vs. wavelength for 3 mm thick double sided polished Ge substrate at 300 K.

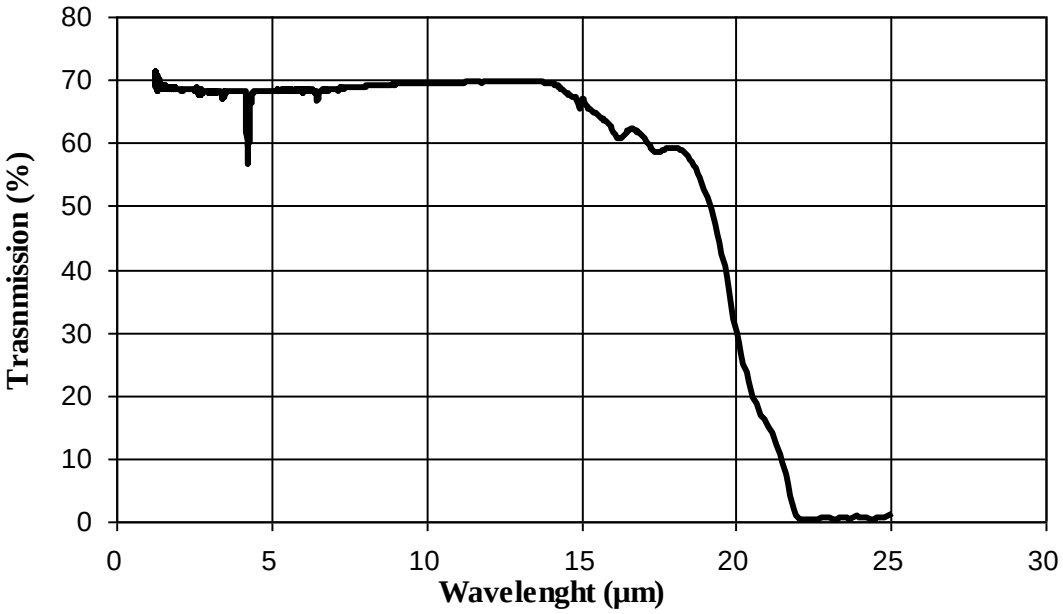

Figure 15. Measured transmission of 3 mm thick ZnSe at 300 K.

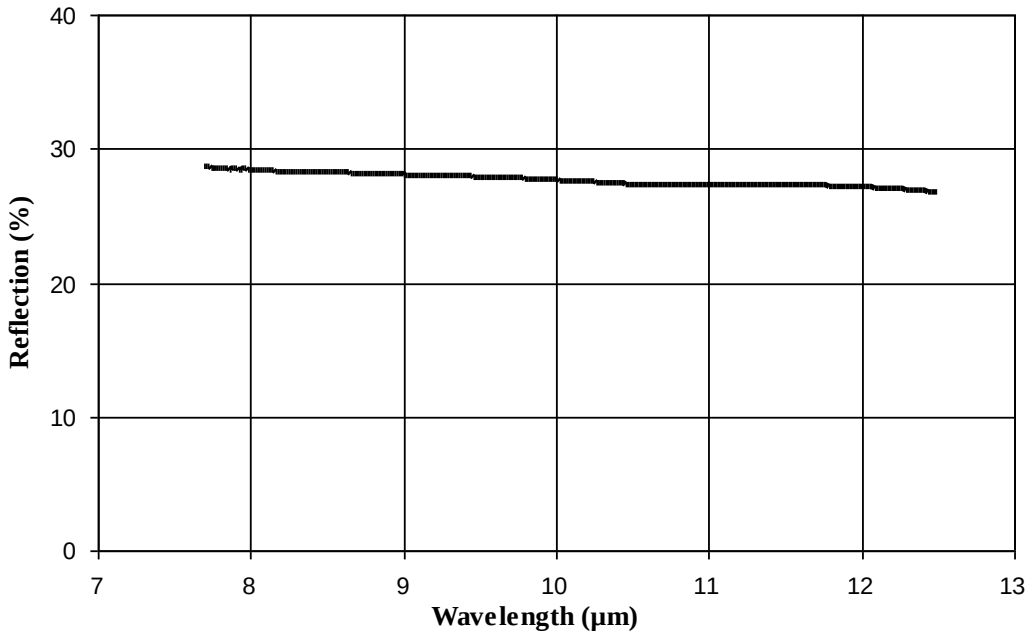

Figure 16. Reflection vs. wavelength for 3 mm thick double-sided polished

ZnSe substrate at 300 K.

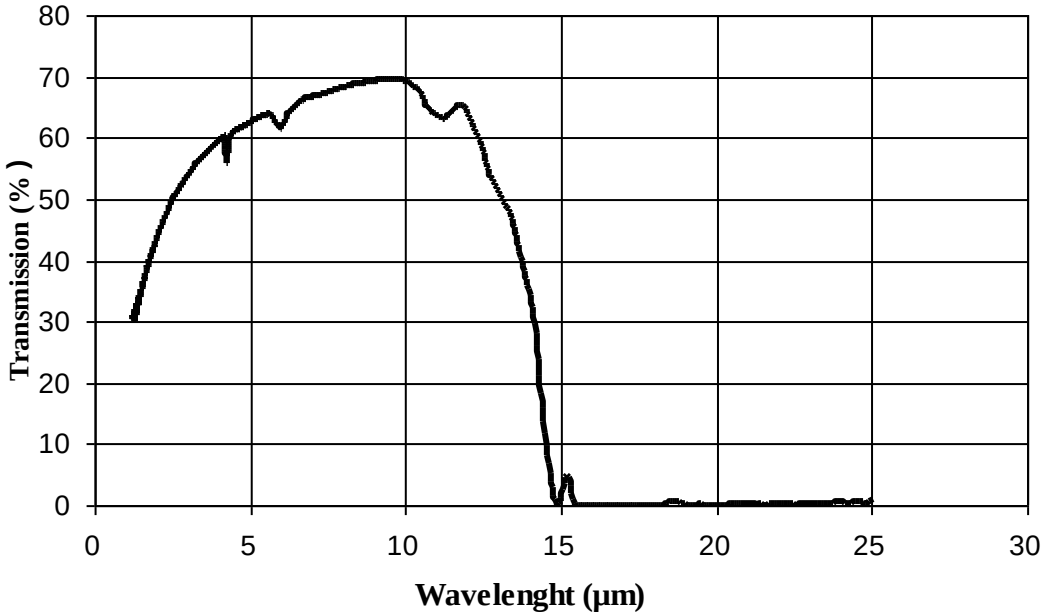

Figure 17. Measured transmission of 3 mm thick ZnS at 300 K.

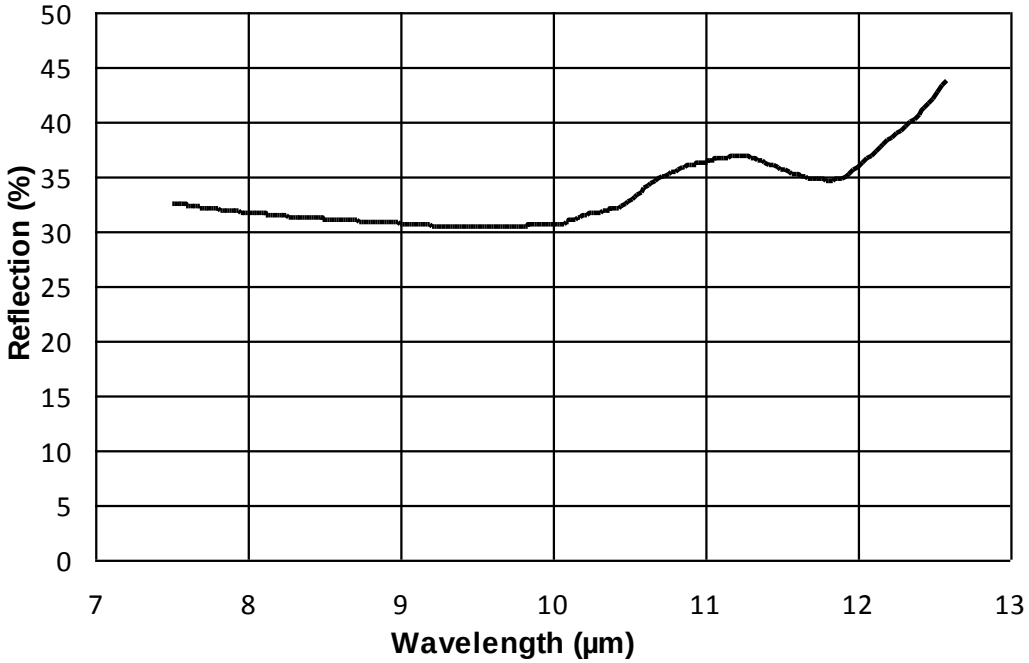

Figure 18. Reflection vs. wavelength for 3 mm thick double-sided polished ZnS substrate at 300 K.

Refractive indices and extinction coefficients of all these substrates are also determined by ellipsometry. J.A. Woollam IR Vase ellipsometer is used. In order to obtain the Brewster angle of each substrate various measurements are carried on around 70º. It is known that at the Brewster angle r_p value of the material should be zero. According to the equation 3.1 at Brewster angle tanΨ should be zero to satisfy the equation. Thus, during the measurement the Brewster angle was searched, that makes tanΨ zero or very close to zero. In Figure 19, it is obvious that, around 76°, psi value is very close to zero.

In Figure 20, calculated refractive indices are given. At 76 °, refractive index is in agreement with reported values. Same measurements have done for the other substrates. Figure 21 and Figure 22 show the Psi values and measured refractive indices at the corresponding measurement angle of ZnS, respectively.

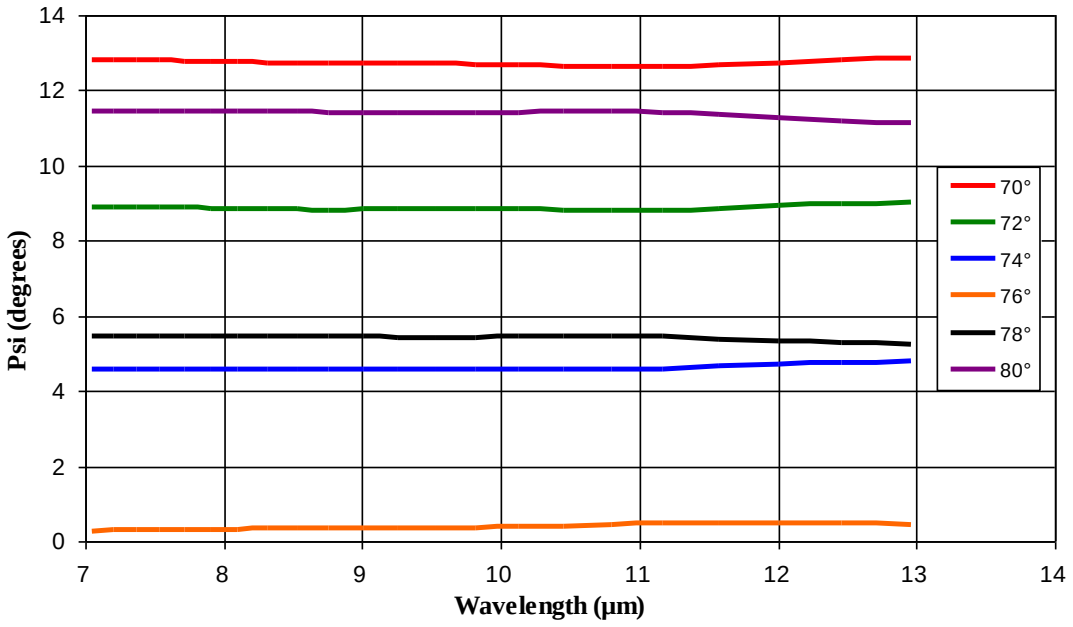

Figure 19. Psi values of germanium.

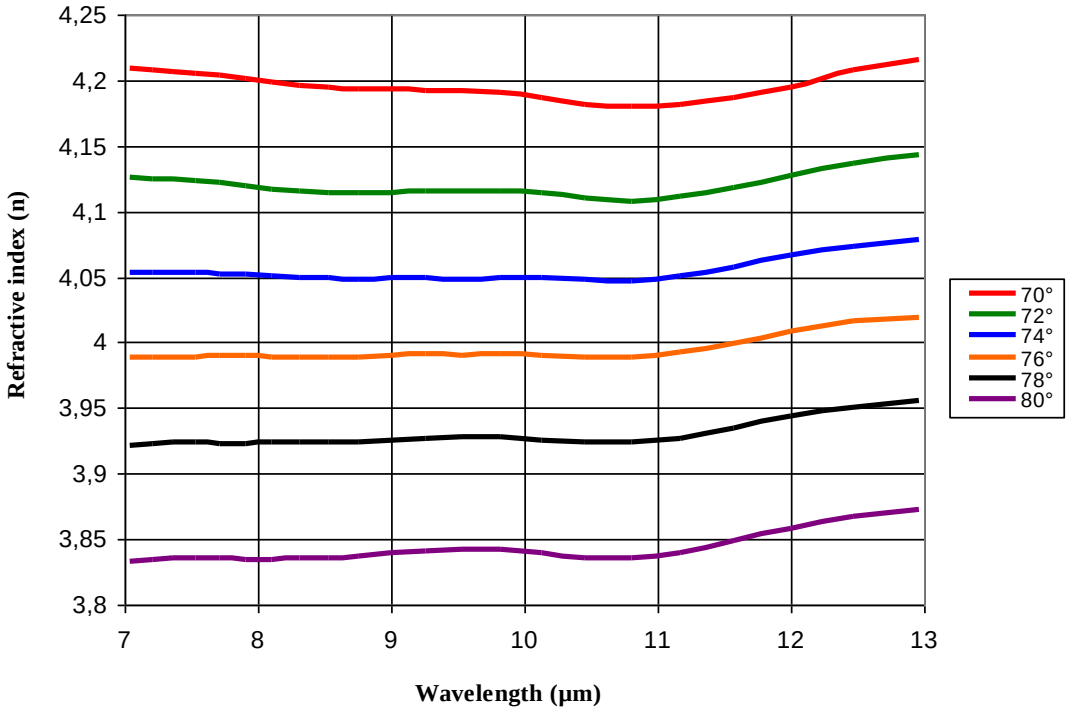

Figure 20. Refractive index values of germanium.

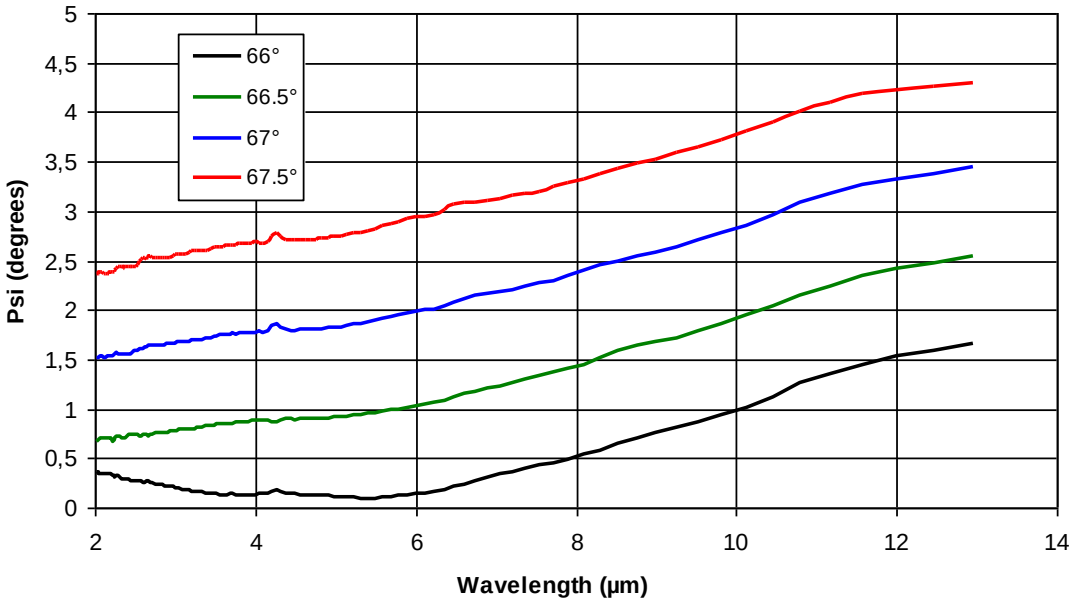

Figure 21. Psi values of zinc sulfide.

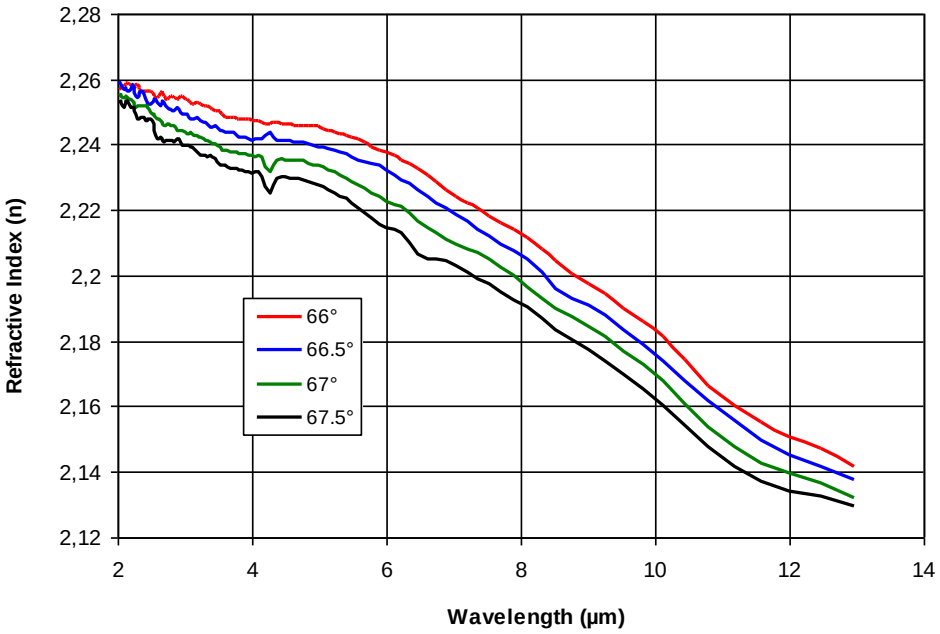

Figure 22. Refractive index values of zinc sulfide.

Figure 23 and Figure 24 show the Psi values and the measured refractive indices at the corresponding measurement angle of ZnSe, respectively.

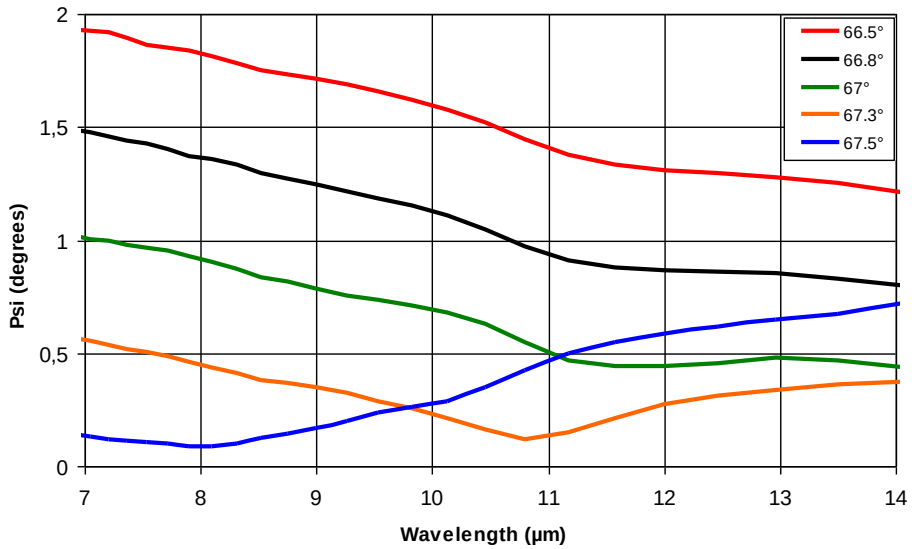

Figure 23. Psi values of zinc selenide.

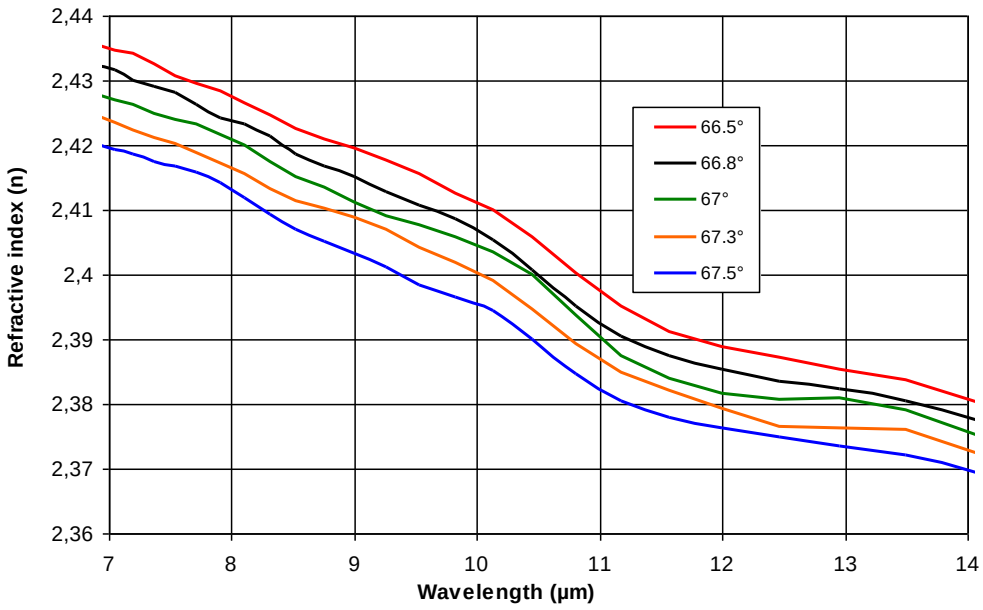

Figure 24. Refractive index values of ZnSe.

The Brewster angles of Ge, ZnS and ZnSe has been found 76°, 66° and 67.5°, respectively. In Figure 25 refractive indices of these substrates at the corresponding angle can be seen.

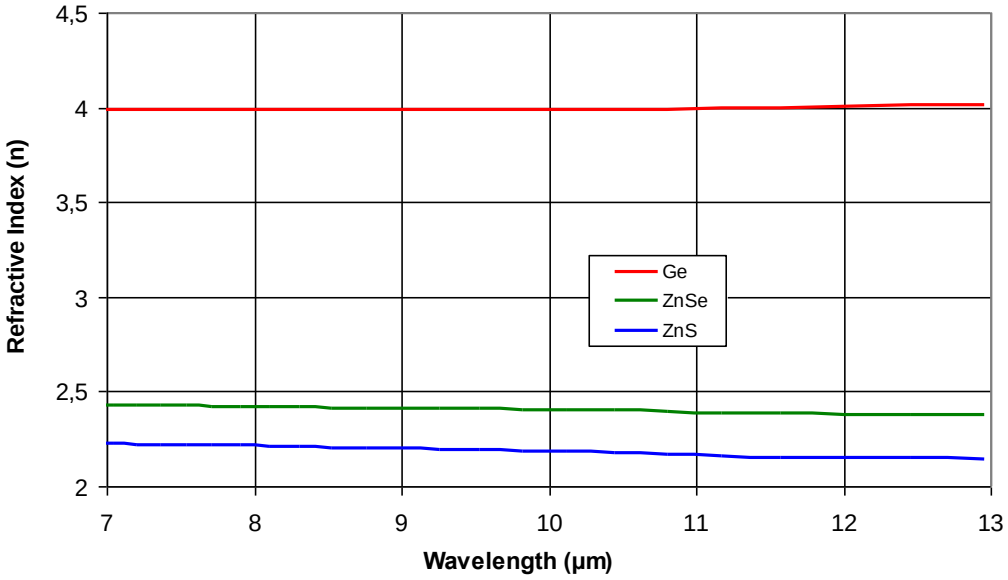

Figure 25. Refractive index values of Ge, ZnSe and ZnS.

However, Figure 25 shows the refractive indexes of all substrate at 300 K. In theory, these curves should fit some well-known refractive index curves like Sellmeir. In Figures 26 to 28, it can be seen that measurement results are in good agreement with the model curves.

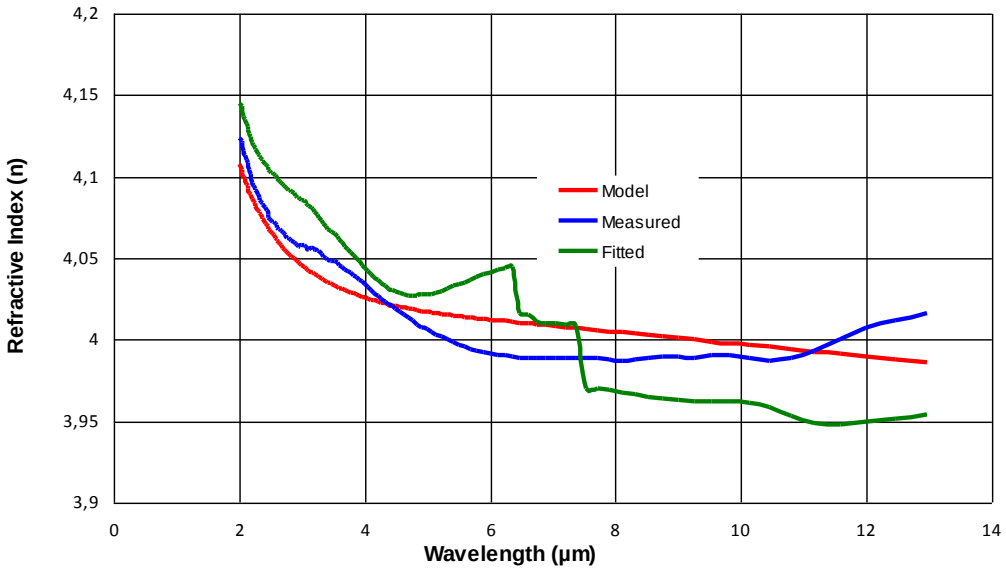

Figure 26. Measured, model and fitted refractive index values of Ge.

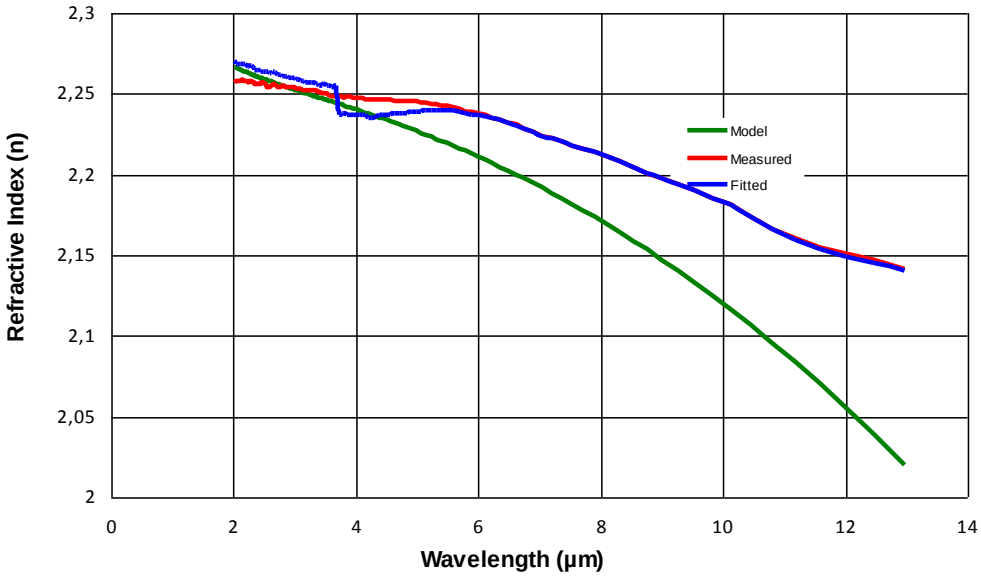

Figure 27. Measured, Model and Fitted Refractive index values of ZnS.

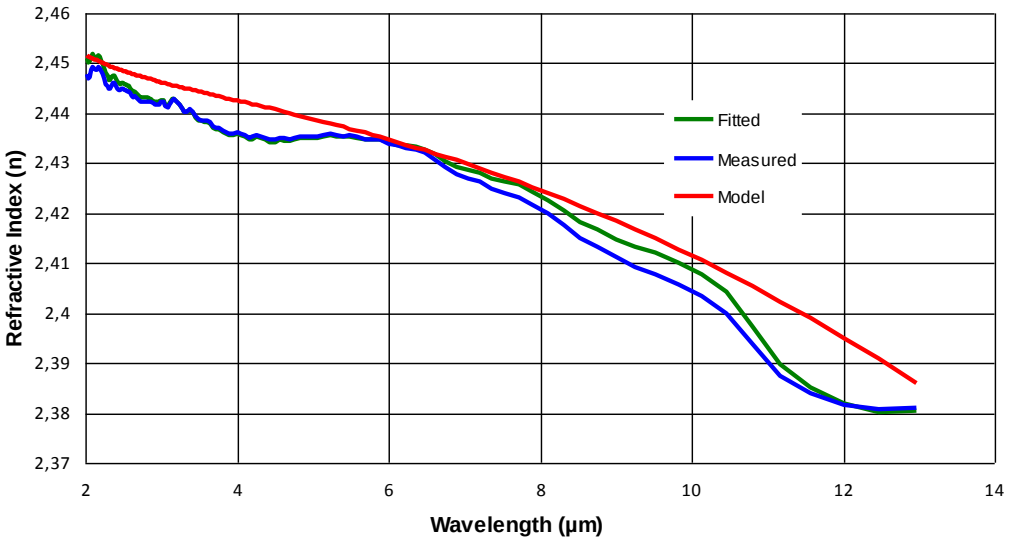

Figure 28. Measured, Model and Fitted Refractive index values of ZnSe.

When fitting data to a model many options are available. For semiconductor materials Sellmeir and Sellmeir-Drude models are generally used fitting methods. According to these models; measured refractive index curves are fitted to the polynomial of the form;

$$n^2 = A + \frac{B\lambda^2}{\lambda^2 - C} + \frac{D\lambda^2}{\lambda^2 - E} \tag{3.2}$$

where A, B, C, D and E are the empirical constants.

3.2. Thickness Measurement and Magnetron Sputtering

Dektak Surface Profiler was used for thickness measurements and its optimization and the PVD Handy Magnetron Sputtering System and the growth conditions for the production of multilayer anti reflecting coatings will be described in here.

3.2.1. Dektak Surface Profiler

The Dektak is a surface profiler that measures step heights, trench depths and roughness on a surface. This is surface contact measurement technique performed by applying a very low force to a stylus which is dragged across trough the surface. Then the change in the force is converted into electrical signals to obtain measured data. The radius of stylus can be range

from 0.2 μm to 25 μm. The radius of stylus determines the lateral resolution. These systems are capable of measuring step heights ranging from 4 angstroms to 1mm [33].

3.2.2. PVD Handy Magnetron Sputtering System and Thickness Optimization

In this work thin film coatings were produced using Vaksis-PVD Handy Magnetron Sputtering System which permits the usage of three targets (see Figure 48). We used 3"x0.125" obtained from Kurt Lesker. The target materials used in this study have the following properties; ZnSe with a purity of 99.9%, contains 44.91% Zn and PbTe with a purity of 99.99%, contains 62.14% Pb.

Even though growth conditions change depending on the coating materials, to give a brief idea, we have tabulated some representative data from our various runs in Table 1.

Table 1. Growth parameters for various runs

	Run #	Initial Vacuum(Torr)	Plasma Vacuum (Torr)	Power (W)	Duration (min)	Avarage Dektak (nm)
ZnSe	1	2,0E-06	5,2E-03	55	30	50
	2	1,0E-06	5,3E-03	100	60	330
	3	1,6E-06	5,3E-03	100	90	430
PbTe	1	1,6E-06	5,5E-03	40	15	60
	2	1,5E-06	5,5E-03	40	60	275
	3	1,6E-06	5,5E-03	40	66	350
	4	1,4E-06	5,5E-03	40	61	330

In order to optimize the system performance for each layer material, many runs have been carried on. During each run power, argon pressure and plasma vacuum were kept almost constant. The thicknesses measured by the thickness monitor were checked by the Dektak measurements. As can be seen from Table 1 the thicknesses indicated by the thickness monitor during the growth and the utilized thicknesses measured by Dektak after the growth differ significantly. For this reason to achieve the required thicknesses instead of using the thickness monitor, duration of the growth is monitored while keeping the deposition conditions constant. Then the time required to deposit the thicknesses shown in Figure 29 is determined to be around 60 min for 360 nm PbTe, 149 min for 730 nm ZnSe and 28 min for

170 nm PbTe. Note that from the experience obtained from several runs, the realized thicknesses slightly increases tough the same target is used in successive growths, therefore in pre determining the growth duration; this phenomenon was taken into account.

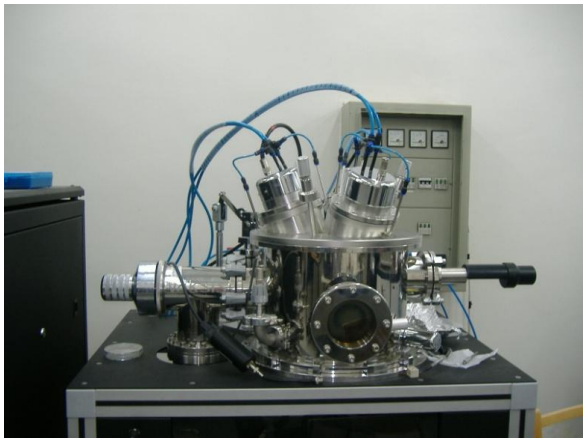

(a)

(b)

Figure 29. (a) PVD Handy Magnetron Sputtering System Chamber, (b) Control unit.

Visual inspection of the produced films by an optical microscope has shown that the films are uniform under a 250X magnification with well defined boundaries. In addition, Dektak

measurements have indicated that the thickness uniformity is acceptable. We have also observed no peeling of the coatings after about six months indicating the well sticking.

3.3. Coating Design and Multilayer Production

At the early stage of a coating design one should state the desired spectral response of that design problem. After that, depending on the problem type the design technique can be chosen. In this work desired performance is determined from the performances of the available anti reflection coatings for the corresponding materials. In the market, transmission values greater than 97 % are quite achievable in the 8-12 µm range for germanium substrates. Thus, obtaining a transmission value not less than 97 % is crucial in this work. Then the design technique and the starting design were determined. Among all the possible design techniques Needle optimization [9] is chosen to obtain a solution to our design problem. With the help of the general starting design approach, the starting layer of low index material with optical thickness of quarter wave is chosen. In our case the low index layer material is ZnSe. Another constraint comes from the minimum achievable physical thickness without loosing the thickness uniformity with the deposition system used. During test deposition runs it was determined that thicknesses below 50 nm for our substrate materials are not reproducible in our system. Thus, this thickness limitation is also added as a "target" of the optimization process. With these starting conditions The Essential Macleod software was used to design a multilayer antireflection coating on germanium substrates. In Figure 29 some of the targets for the spectral performance of the coating are shown. According to the Figure 29 transmittance greater than or equal to 97 % is entered in 8-12µm range with tolerance of ± 1 %. The wavelength increment is chosen as 25 nm. Note that in Figure 30 only a very small portion of the target input page is shown since it is too long to present here.

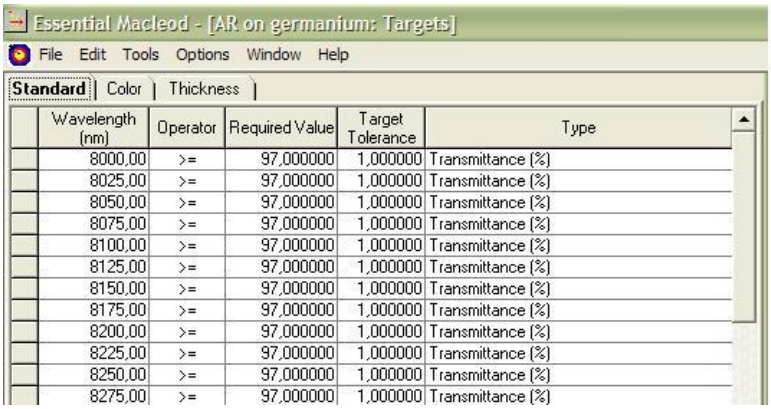

Wavelength (nm)	Operator	Required Value	Target Tolerance	Type
8000,00	>=	97,000000	1,000000	Transmittance (%)
8025,00	>=	97,000000	1,000000	Transmittance (%)
8050,00	>=	97,000000	1,000000	Transmittance (%)
8075,00	>=	97,000000	1,000000	Transmittance (%)
8100,00	>=	97,000000	1,000000	Transmittance (%)
8125,00	>=	97,000000	1,000000	Transmittance (%)
8150,00	>=	97,000000	1,000000	Transmittance (%)
8175,00	>=	97,000000	1,000000	Transmittance (%)
8200,00	>=	97,000000	1,000000	Transmittance (%)
8225,00	>=	97,000000	1,000000	Transmittance (%)
8250,00	>=	97,000000	1,000000	Transmittance (%)
8275,00	>=	97,000000	1,000000	Transmittance (%)

Figure 30. Spectral targets for optimization.

In Figure 31 starting design is shown. Reference wavelength appearing here is the design wavelength of the coating; 10 μm. Germanium and ZnSe seen in the figure are the substrate and the layer material, respectively.

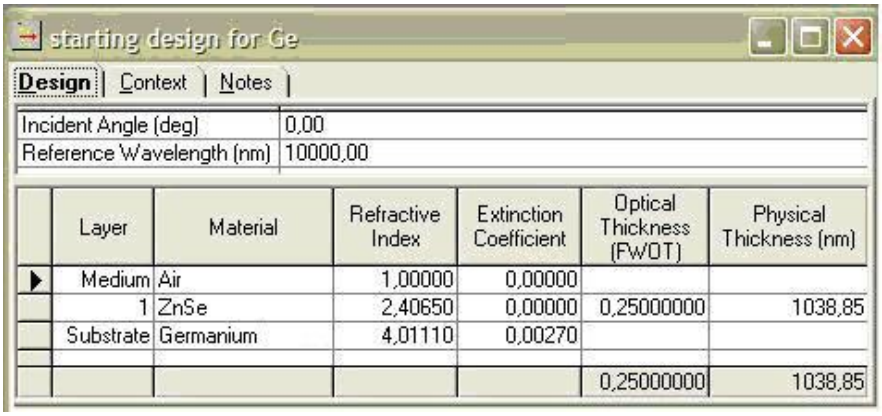

Incident Angle (deg)	0,00
Reference Wavelength (nm)	10000,00

Layer	Material	Refractive Index	Extinction Coefficient	Optical Thickness (FWOT)	Physical Thickness (nm)
Medium	Air	1,00000	0,00000		
1	ZnSe	2,40650	0,00000	0,25000000	1038,85
Substrate	Germanium	4,01110	0,00270		
				0,25000000	1038,85

Figure 31. Starting design for a germanium substrate.

Another important window of the software is the Needle synthesis parameters window. This is shown in Figure 32.

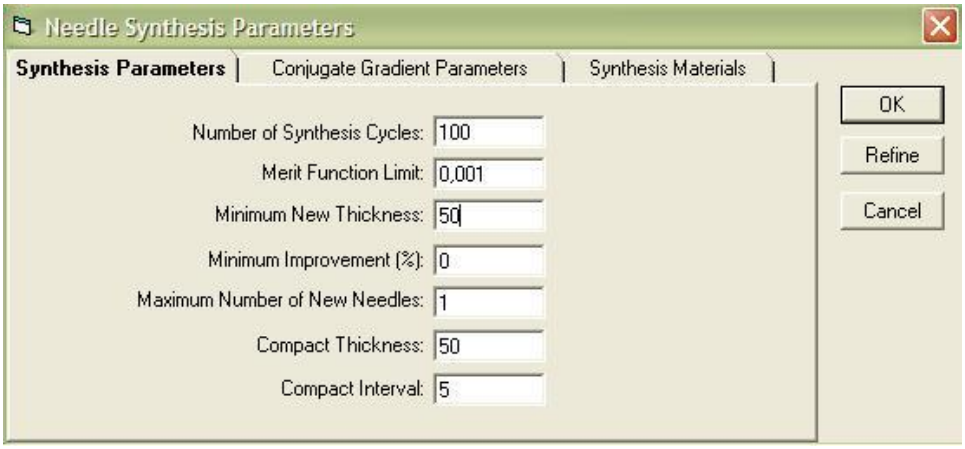

Figure 32. Needle Synthesis parameters window.

Definitions of the design parameters seen in Figure 32 are the followings;

Number of Synthesis Cycles: The number of times that Needle Synthesis will attempt to add layers.

Merit Function Limit: When the merit figure falls below this value, Needle Synthesis will stop.

Minimum New Thickness: When, after the refinement phase completes, the new layers are thinner than this value, Needle Synthesis will add material to one end of the design to provide extra space for layer insertion.

Minimum Improvement: When, after the refinement phase completes, the merit figure has reduced by this proportion, Needle Synthesis will add material to one end of the design to provide extra space for layer insertion.

Maximum Number of New Needles: The maximum number of new layers added at a time.

When Compact Interval is greater than zero, during each Compact Interval Iteration, Needle Synthesis will compact the design, removing layers whose thicknesses are less than Compact Thickness. If Compact Interval is zero, then the design is never compacted. Minimum New Thickness and Compact Thickness are always in units of nanometers [21].

The design obtained with the minimum figure of merit and its transmittance is shown in Figures 33 and 34, respectively.

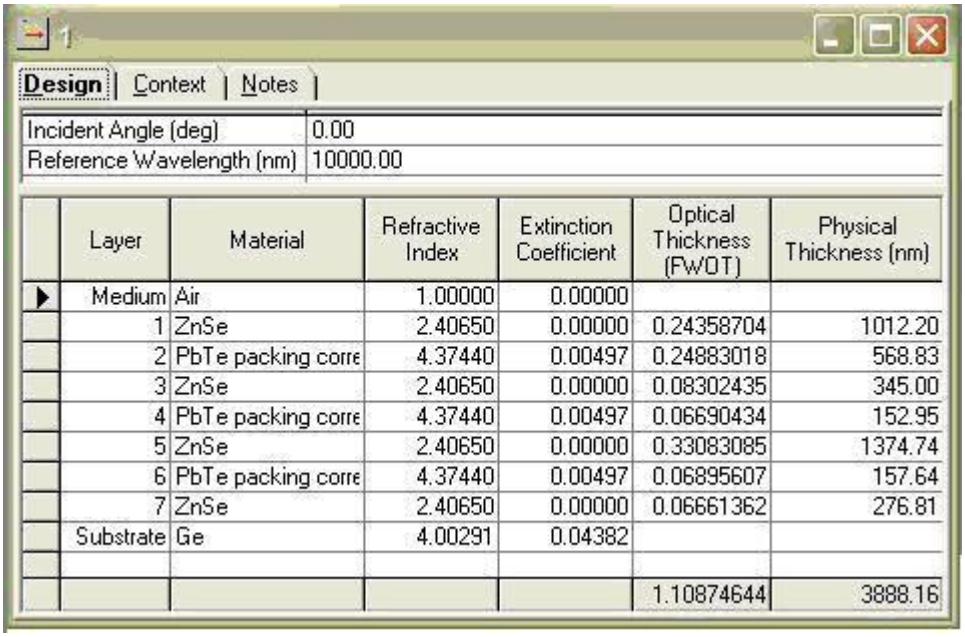

1

Design | Context | Notes

Incident Angle (deg)	0.00
Reference Wavelength (nm)	10000.00

	Layer	Material	Refractive Index	Extinction Coefficient	Optical Thickness (FWOT)	Physical Thickness (nm)
▶	Medium	Air	1.00000	0.00000		
	1	ZnSe	2.40650	0.00000	0.24358704	1012.20
	2	PbTe packing corre	4.37440	0.00497	0.24883018	568.83
	3	ZnSe	2.40650	0.00000	0.08302435	345.00
	4	PbTe packing corre	4.37440	0.00497	0.06690434	152.95
	5	ZnSe	2.40650	0.00000	0.33083085	1374.74
	6	PbTe packing corre	4.37440	0.00497	0.06895607	157.64
	7	ZnSe	2.40650	0.00000	0.06661362	276.81
	Substrate	Ge	4.00291	0.04382		
					1.10874644	3888.16

Figure 33. Final AR design for germanium substrate.

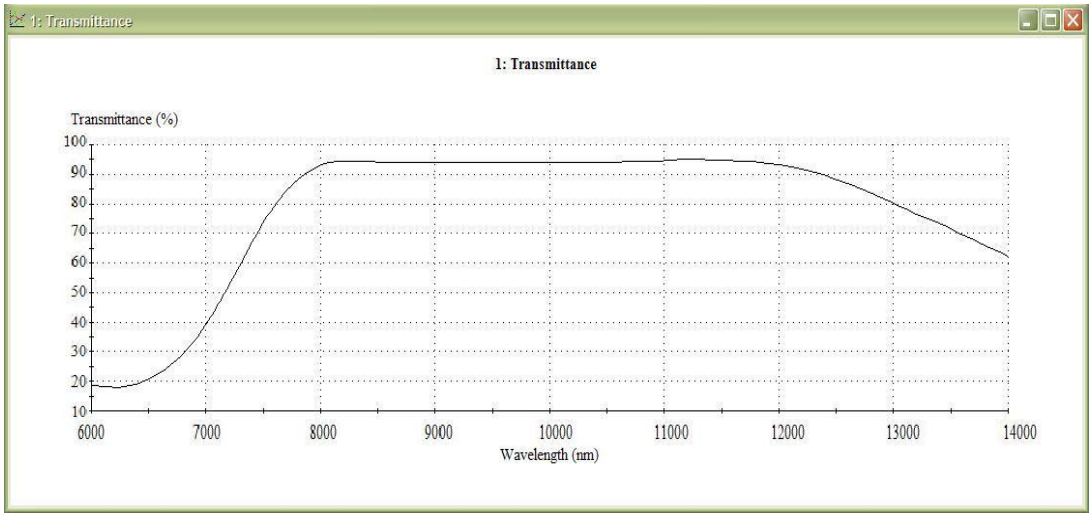

Figure 34. Transmittance of 3 mm thick germanium substrate, coated on both sides.

Note that the transmittance curve shown in Figure 34 belongs to a 3 mm thick germanium sample which has the coating shown in Figure 33 on both sides. Similar work will be done for the other substrate materials.

However, in our coating system, it is not possible to coat large numbers of thick layers since the chimney around the targets are also coated during the deposition and at some point they become insulator resulting in the loss of plasma. Thus, in the present work, the spectrum was narrowed down to 9.7-10.3 µm range from 8-12 µm. This enables us to design an AR coating with less number of layer while still giving chance to verify our design and production ability.

To do this, ZnS was chosen to be the substrate material, whereas the ZnSe and PbTe were used as the low and high index materials in the coating design. After choosing a single thick layer of ZnSe as a starting design and introducing the target parameters, the Needle optimization session was started. In Figure 35, target parameters that determine the desired transmission values in the corresponding region can be seen.

ZnS uzeri multilayer2- ZnS2: Targets

Standard | Color | Thickness |

Wavelength (nm)	Operator	Required Value	Target Tolerance	Type
9700,00	>=	95,000000	1,000000	Transmittance (%)
9725,00	>=	95,000000	1,000000	Transmittance (%)
9750,00	>=	95,000000	1,000000	Transmittance (%)
9775,00	>=	95,000000	1,000000	Transmittance (%)
9800,00	>=	95,000000	1,000000	Transmittance (%)
9825,00	>=	95,000000	1,000000	Transmittance (%)
9850,00	>=	95,000000	1,000000	Transmittance (%)
9875,00	>=	95,000000	1,000000	Transmittance (%)
9900,00	>=	95,000000	1,000000	Transmittance (%)
9925,00	>=	95,000000	1,000000	Transmittance (%)
9950,00	>=	95,000000	1,000000	Transmittance (%)
9975,00	>=	95,000000	1,000000	Transmittance (%)
10000,00	>=	95,000000	1,000000	Transmittance (%)
10025,00	>=	95,000000	1,000000	Transmittance (%)
10050,00	>=	95,000000	1,000000	Transmittance (%)
10075,00	>=	95,000000	1,000000	Transmittance (%)
10100,00	>=	95,000000	1,000000	Transmittance (%)
10125,00	>=	95,000000	1,000000	Transmittance (%)
10150,00	>=	95,000000	1,000000	Transmittance (%)
10175,00	>=	95,000000	1,000000	Transmittance (%)
10200,00	>=	95,000000	1,000000	Transmittance (%)
10225,00	>=	95,000000	1,000000	Transmittance (%)
10250,00	>=	95,000000	1,000000	Transmittance (%)
10275,00	>=	95,000000	1,000000	Transmittance (%)
10300,00	>=	95,000000	1,000000	Transmittance (%)

Figure 35. Optimization targets of ZnS substrate.

After optimization the design shown in Figure 36 was achieved. The corresponding transmission curve of double sided coated substrate is shown in Figure 37.

ZnS1

Design | Context | Notes

Incident Angle (deg)	0,00
Reference Wavelength (nm)	10000,00

	Layer	Material	Refractive Index	Extinction Coefficient	Optical Thickness (FWOT)	Physical Thickness (nm)
▶	Medium	Air	1,00000	0,00000		
	1	PbTe	5,56000	0,00497	0,10564000	190,00
	2	ZnSe	2,40650	0,00000	0,10588600	440,00
	3	PbTe	5,56000	0,00497	0,16680000	300,00
	Substrate	ZnS begum	2,18316	0,00343		
					0,37832600	930,00

Figure 36. Coating design on ZnS substrate operating in 9.7-10.3 µm region.

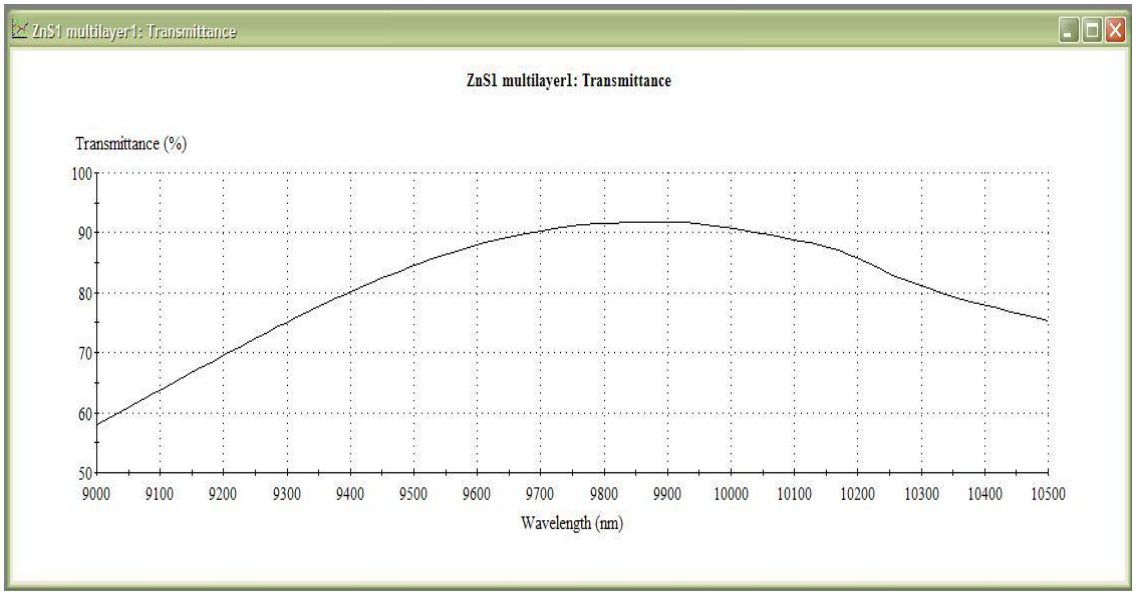

Figure 37. Transmission of coated ZnS in 9.7-10.3 µm region.

Finally, the experimentally obtained transmission spectrum is given with that of obtained from The Essential Macleod for comparison in Figure 38.

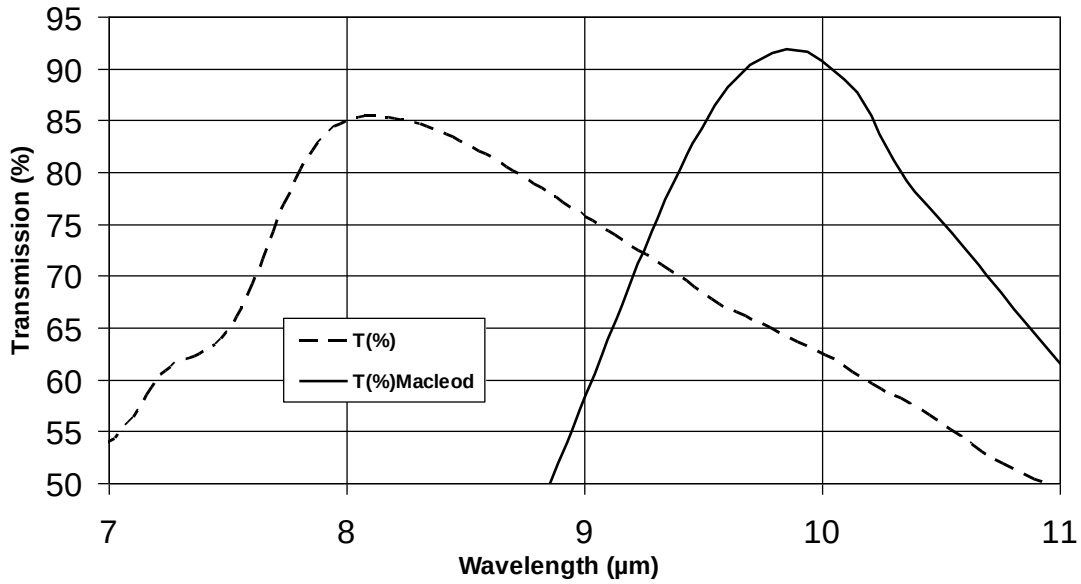

Figure 38. Transmission vs. wavelength plots for deposited and theoretical multilayers.

The dashed curve shows the transmission of the produced coating whereas the solid one shows the theoretical curve obtained from The Essential Macleod. The discrepancy of the peak positions of the curves is noticeable. Produced multilayer has its maximum around 8 µm which is shifted toward the short wavelengths as compared to The Essential Macleod's design. During single layer studies of each layer materials it is also observed that the PbTe shows the similar shift in its transmittance spectrum (see Figure 40). It should be noted that ZnSe's matches with the theoretical transmission curve as shown in Figure 38.

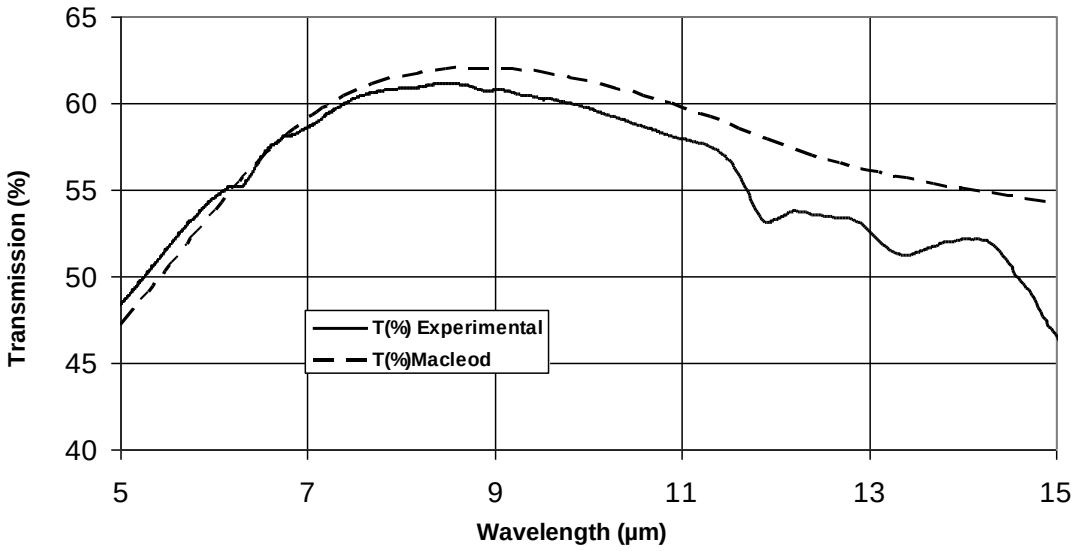

Figure 39. Transmission vs. wavelength plots for 880 nm ZnSe on Ge substrate.

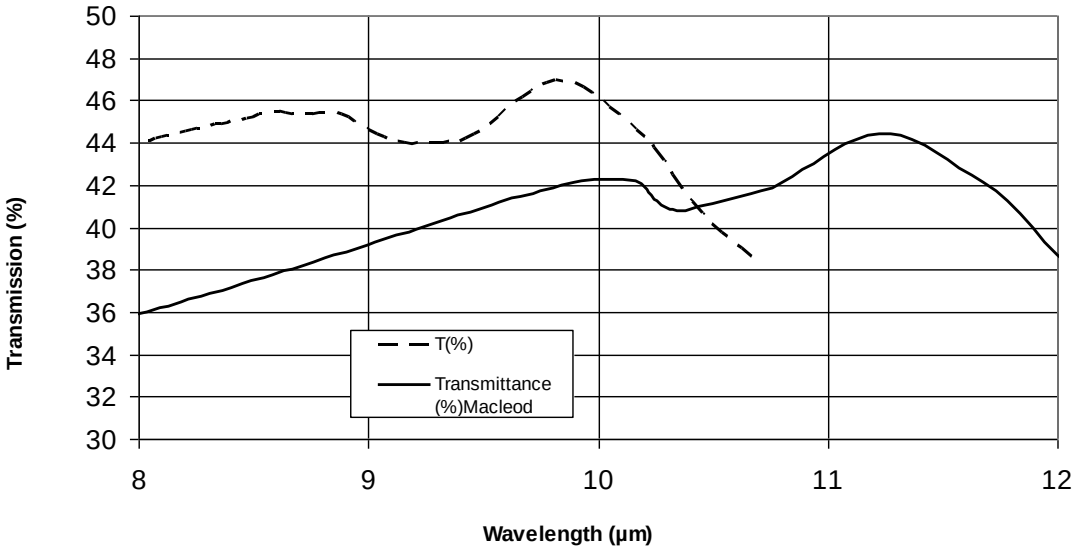

Figure 40. Transmission vs. wavelength of deposited and theoretical 350 nm PbTe on ZnS substrate.

The observed shifts may be the result of two possible reasons. The first one is that the deposited layers' thicknesses are not the desired ones. And the second one is that the refractive indices do not have the same theoretical values used in the calculations. In our

situation the former most probably may not be the case, since, the deposition rates and the produced thickness' are confirmed several times during thickness optimization processes (see Section 3.3.2). Then it is concluded that the shift is due to difference of the realized dispersion properties of the layer materials than the values extracted from the library of the software. At that point it is necessary to introduce the concept of "Packing Density".

Thin films produced by several techniques have a granular or columnar structure. Such microstructures are porous in nature and therefore have lower packing densities. The reduction in the packing density affects many physical properties of the thin films including the optical properties. From the mechanical point of view low density packing degrades the stability due to environmental influence, [22, 23]. The most commonly observed optical changes due to low packing density result in the decreasing value of refractive index and the increasing absorption [24].

The packing density is defined as the ratio of the volume of solid part of film to the total volume the film. Ideally for non porous structure packing density must be unity. However, in practice for optical films grown by various techniques packing densities varying from 0.6 to 1.0 were reported in literature [25-27]. Depending on the type of material and growth technique, various methods have been proposed to increase the packing density in thin film coatings. For example, sputtering pressure, substrate temperature, annealing, oxidation, argon ion bombardment have been used to monitor the packing density [28-31].

The dependence of the refractive index to the packing density p can be expressed in its simplest form as

$$n = pn_s(1-p)n_v \tag{3.3}$$

where n_s and n_v refer to refractive index of the solid part and that of the voids, respectively. However, this formula holds true for low index materials, mostly for n<2. Since for the coating materials used in this thesis refractive index around 10 μm is much higher , a relation corresponding to equation A due to Harris et al. [32] must be considered;

$$n^2 = \frac{(1-p)n_v^4 + (1+p)n_v^2 n_s^2}{(1+p)n_v^2 + (1-p)n_s^2} \quad n^2 = \frac{(1-p)n_v{}^4 + (1+p)n_v{}^2 n_s{}^2}{(1+p)n_v{}^2 + (1-p)n_v{}^2} pn_s(1-p)n_v \tag{3.4}$$

The approximate packing density can be obtained by using the quite well established theoretical background values with some experimental methods. However, this is beyond the scope of this thesis work. On the other hand, from the comparison of transmittance spectrum of the grown structures and the theoretical transmittance spectrum of the multilayer structure based on the The Essential Macleod' library, it is concluded that the refinement of the refractive index, then the reoptimization of the design is required. We have attributed the variations in index to the changes in packing density. For this purpose we have applied a so called "reverse engineering" method. The transmission spectra of our samples were compared with those proposed by Macleod simulations created for various packing densities. The packing density, corresponding to Macleod spectra that matches best with the experimentally obtained transmission spectra, is taken as the representative packing density value for our coatings. The recalculation of the refractive index values were then based on this packing value. With this approach we have successfully produced double sided AR coatings on ZnS substrates with more than 80% transmission in the 9.5-10.5 μm range. The procedure explained here is applied on 3-layer AR coating on ZnS. Figure 41 shows the change in the transmission spectrum of the coating with changing packing densities and its comparison with the experimental values.

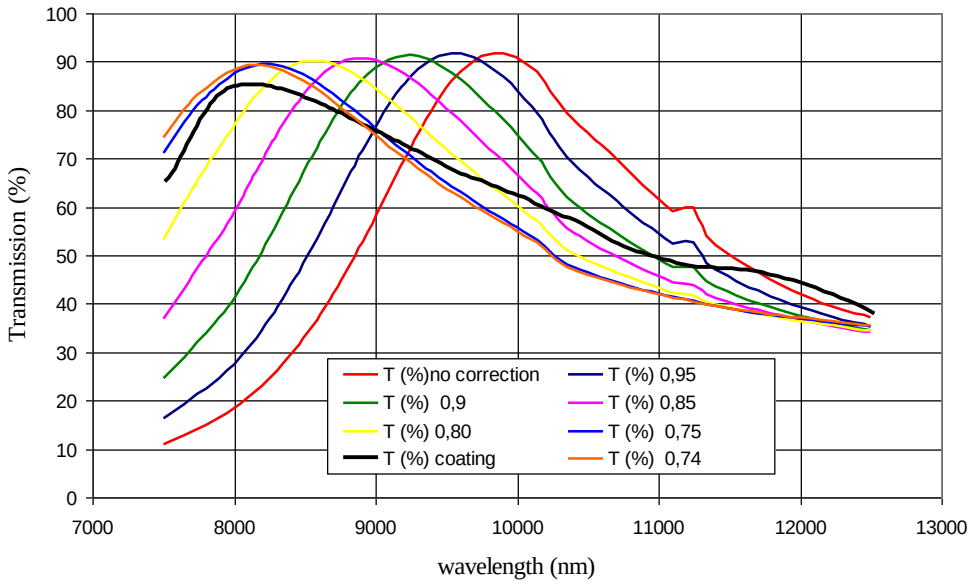

Figure 41. Transmission vs. wavelength for different packing density values and for deposited coating.

When we examine closely, transmission values are very close to the calculated one for 0.74 packing density values. With the help of this information the refractive index values for the 0.74 packing density are recalculated. In Figure 42, the refractive index values in the library and the corrected ones can be seen.

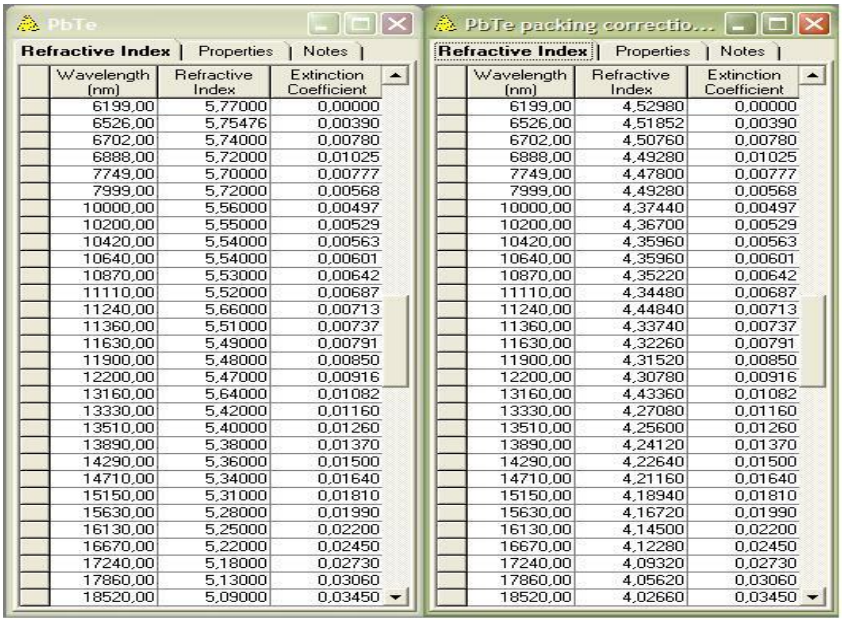

PbTe

Refractive Index | Properties | Notes

Wavelength (nm)	Refractive Index	Extinction Coefficient
6199,00	5,77000	0,00000
6526,00	5,75476	0,00390
6702,00	5,74000	0,00780
6888,00	5,72000	0,01025
7749,00	5,70000	0,00777
7999,00	5,72000	0,00568
10000,00	5,56000	0,00497
10200,00	5,55000	0,00529
10420,00	5,54000	0,00563
10640,00	5,54000	0,00601
10870,00	5,53000	0,00642
11110,00	5,52000	0,00687
11240,00	5,66000	0,00713
11360,00	5,51000	0,00737
11630,00	5,49000	0,00791
11900,00	5,48000	0,00850
12200,00	5,47000	0,00916
13160,00	5,64000	0,01082
13330,00	5,42000	0,01160
13510,00	5,40000	0,01260
13890,00	5,38000	0,01370
14290,00	5,36000	0,01500
14710,00	5,34000	0,01640
15150,00	5,31000	0,01810
15630,00	5,28000	0,01990
16130,00	5,25000	0,02200
16670,00	5,22000	0,02450
17240,00	5,18000	0,02730
17860,00	5,13000	0,03060
18520,00	5,09000	0,03450

PbTe packing correctio...

Refractive Index | Properties | Notes

Wavelength (nm)	Refractive Index	Extinction Coefficient
6199,00	4,52980	0,00000
6526,00	4,51852	0,00390
6702,00	4,50760	0,00780
6888,00	4,49280	0,01025
7749,00	4,47800	0,00777
7999,00	4,49280	0,00568
10000,00	4,37440	0,00497
10200,00	4,36700	0,00529
10420,00	4,35960	0,00563
10640,00	4,35960	0,00601
10870,00	4,35220	0,00642
11110,00	4,34480	0,00687
11240,00	4,44840	0,00713
11360,00	4,33740	0,00737
11630,00	4,32260	0,00791
11900,00	4,31520	0,00850
12200,00	4,30780	0,00916
13160,00	4,43360	0,01082
13330,00	4,27080	0,01160
13510,00	4,25600	0,01260
13890,00	4,24120	0,01370
14290,00	4,22640	0,01500
14710,00	4,21160	0,01640
15150,00	4,18940	0,01810
15630,00	4,16720	0,01990
16130,00	4,14500	0,02200
16670,00	4,12280	0,02450
17240,00	4,09320	0,02730
17860,00	4,05620	0,03060
18520,00	4,02660	0,03450

Figure 42. Refractive index of PbTe before and after packing correction.

Using the corrected PbTe as the high index material, re-optimization of the design was carried on. In Figures 43 and 44, the new thicknesses of the new design and its corresponding transmission values are given, respectively. And also, in Figure 45 transmission curves of deposited and calculated multilayers are shown.

ZnS2

Design | Context | Notes |

Incident Angle (deg)	0,00
Reference Wavelength (nm)	10000,00

	Layer	Material	Refractive Index	Extinction Coefficient	Optical Thickness (FWOT)	Physical Thickness (nm)
▶	Medium	Air	1,00000	0,00000		
	1	PbTe packing corre	4,37440	0,00497	0,07436480	170,00
	2	ZnSe	2,40650	0,00000	0,17567451	730,00
	3	PbTe packing corre	4,37440	0,00497	0,15747839	360,00
	Substrate	ZnS begum	2,18316	0,00343		
					0,40751770	1260,00

Figure 43. The new design after the packing correction.

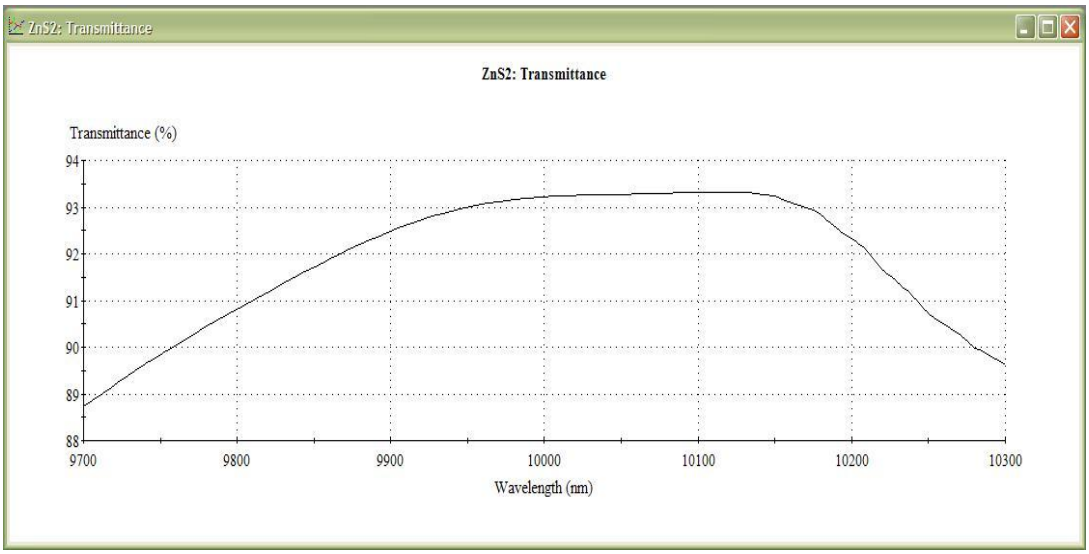

Figure 44. Transmittance of the new design.

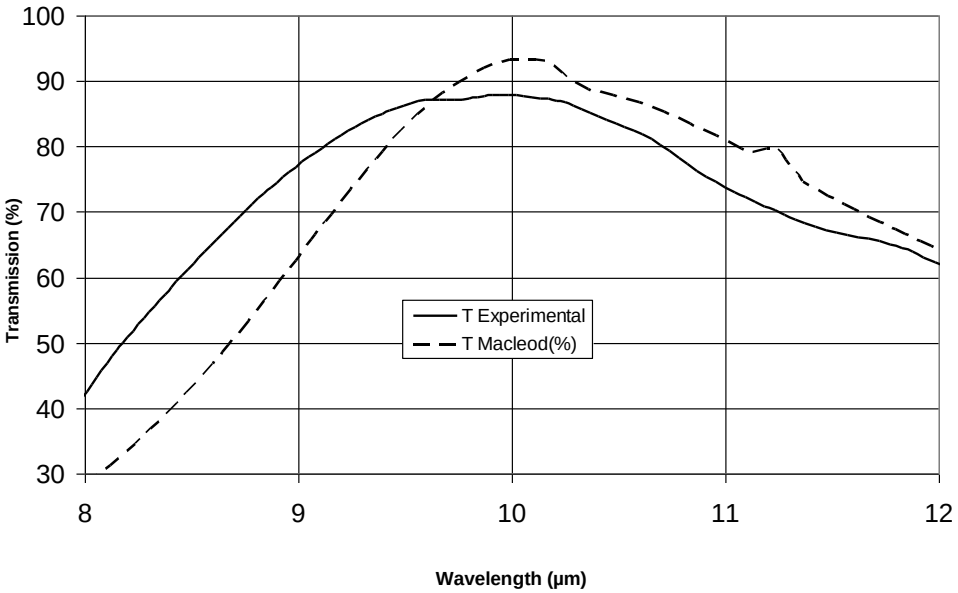

Figure 45. Deposited and calculated transmission of AR coated ZnS.

Similar studies were done for Germanium substrates. Coating design optimization with proper optimization targets yield the design operating in 9.7 to 10.3 µm region, shown in Figure 46. Since similar optimization procedure was used for Germanium the related information will not be repeated here. In Figures 47 and 48, the calculated transmission curve and its comparison with the utilized one are given, respectively.

Ge2

Design | Context | Notes

Incident Angle (deg)	0.00
Reference Wavelength (nm)	10000.00

	Layer	Material	Refractive Index	Extinction Coefficient	Optical Thickness (FWOT)	Physical Thickness (nm)
▶	Medium	Air	1.00000	0.00000		
	1	PbTe packing corre	4.37440	0.00497	0.02624640	60.00
	2	ZnSe	2.40650	0.00000	0.18289401	760.00
	Substrate	Ge begum	4.00291	0.04382		
					0.20914041	820.00

Figure 46. Coating design on Ge substrate operating in 9.7-10.3µm region.

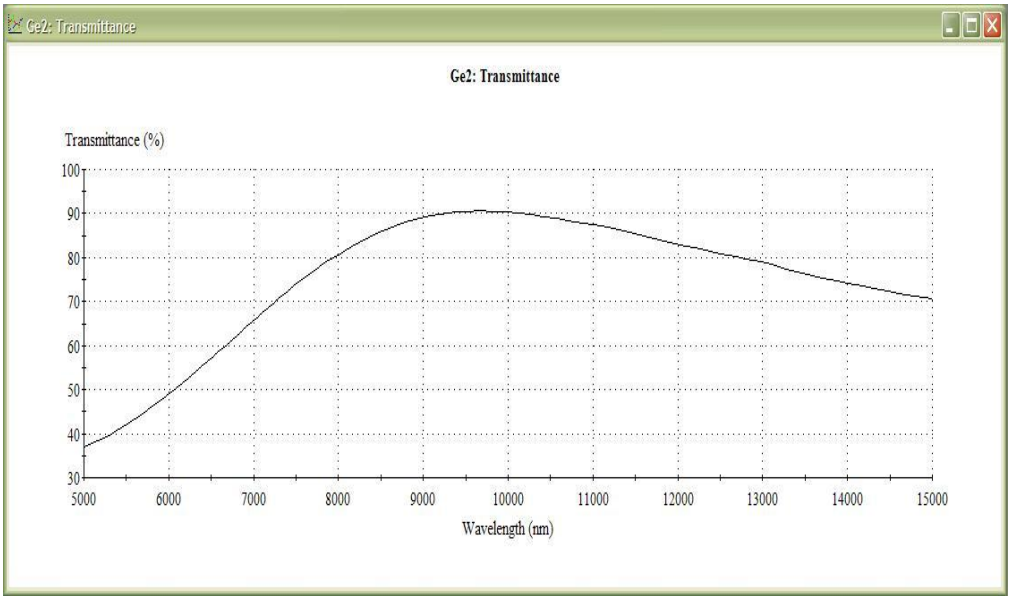

Figure 47. Transmittance of calculated multilayer on Ge.

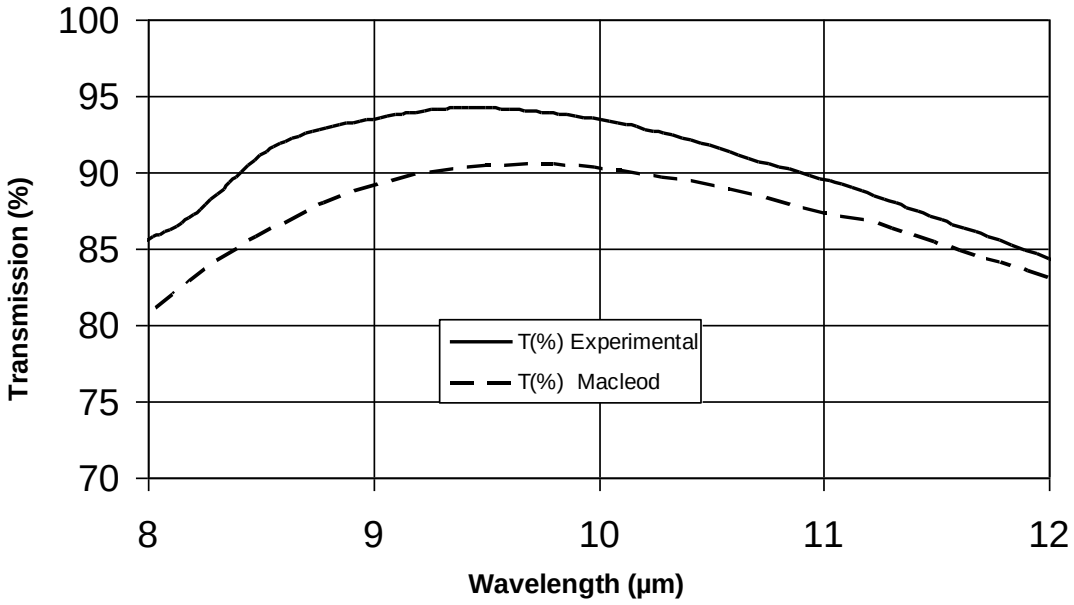

Figure 48. Deposited and calculated transmission of AR coated Ge.

CHAPTER 4

RESULTS AND DISCUSSIONS

In this thesis, we have investigated the transmission characteristics of multilayer coatings on Ge, ZnS and ZnSe substrates. To achieve the optimum highest transmission in 8-12 μm wavelength region the optical properties of all the constituents, substrates as well as the thin film coating layers, must be known. For this purpose ellipsometry and FTIR are used for the substrate materials. The required parameters for the layer materials have been taken from the library of the software used for multilayer coating design. Finally, the multilayer coated structure was produced, as based on the results of the optimized design, by magnetron sputtering method and the success of the optimization and deposition technique has been tested by FTIR measurements.

One possible reason of the experimental uncertainties is the absorption losses. This certainly adds some uncertainty to the calculated results in the design and optimization. Other sources of uncertainties are the instrumental errors, sensitivity of the instruments, systematic and random thickness errors. Finally, errors arising from not exact values of the refractive indices and dispersion should also be taken into account.

The experimentally obtained parameters of the substrate materials required for the design and optimization are given below.

In Figures 13 and 14 measured transmissions and reflection spectra of a 3 mm thick germanium substrate are shown respectively. It has been observed that in 2-11μm range germanium has almost constant transmission around 45 %. This value is quite consistent with those reported in literature [5, 34, 35]. On samples refractive index and extinction coefficient measurements were also carried out with an infrared ellipsometer. In order to determine the Brewster angle a series of measurements were performed around the pseudo-Brewster angle and it is found as 76° for germanium. This angle is also consistent with the tabulated values for the commercially available germanium products [36]. Using the data obtained from the ellipsometer measurements calculated refractive indices at pseudo-Brewster angle and at the Brewster angle are shown in Figure 20 for the germanium sample. It is obvious that the refractive index approaches the values (around 4 in between 7-12 μm range) given in the literature [37, 38].

The same measurements and analysis described above for germanium are repeated for ZnS and ZnSe. Transmission values are around 60-70% (5-12 μm) for ZnS and 70% (2-15 μm) for ZnSe. The observed refractive index values lie in the range 2.26-2.14 for ZnS and 2.15-2.38 for ZnSe in the wavelength region of 2-13 μm. These values are in accordance with those tabulated in Ref. [34].

According to the preliminary design and optimization procedures, it is observed that the spectral performance is getting better with increasing number of layers. According to the Figure 33 with 7- layer AR coating on germanium substrate has given the desired spectral response in 8-12 μm range. However, some of the low index material layers were found to be too thick to be realized in our coating system. In order to overcome this problem, number of layers should be increased. This fact holds true for the other substrate materials. While designing the AR coating for ZnS and ZnSe we have used different approach. Their optical properties in the corresponding region are almost similar. Therefore, it is possible to design for both materials. That enables us to coat both materials in the same run providing an economical mass production [39]. The coating design seen in Figure 49 can be an example of such a coating in 8-12 μm range. And its corresponding transmission curve is given in Figure 50.

ZnS and ZnSe

Design | Context | Notes

Incident Angle (deg)	0.00
Reference Wavelength (nm)	10000.00

	Layer	Material	Refractive Index	Extinction Coefficient	Optical Thickness (FWOT)	Physical Thickness (nm)
	Medium	Air	1.00000	0.00000		
	1	ZnSe	2.40650	0.00000	0.25414393	1056.07
	2	PbTe packing corre	4.37440	0.00497	0.18758829	428.83
	3	ZnSe	2.40650	0.00000	0.49348333	2050.63
	4	PbTe packing corre	4.37440	0.00497	0.19813707	452.95
	5	ZnSe	2.40650	0.00000	0.05956572	247.52
	6	PbTe packing corre	4.37440	0.00497	0.05676591	129.77
	7	ZnSe	2.40650	0.00000	0.39575728	1644.53
	8	PbTe packing corre	4.37440	0.00497	0.38690396	884.47
	9	ZnSe	2.40650	0.00000	0.04801583	199.53
▶	10	PbTe packing corre	4.37440	0.00497	0.05897065	134.81
	Substrate		2.18316	0.00343		
					2.13933197	7229.11

Figure 49. AR Coating design for both ZnS and ZnSe in 8-12 μm range.

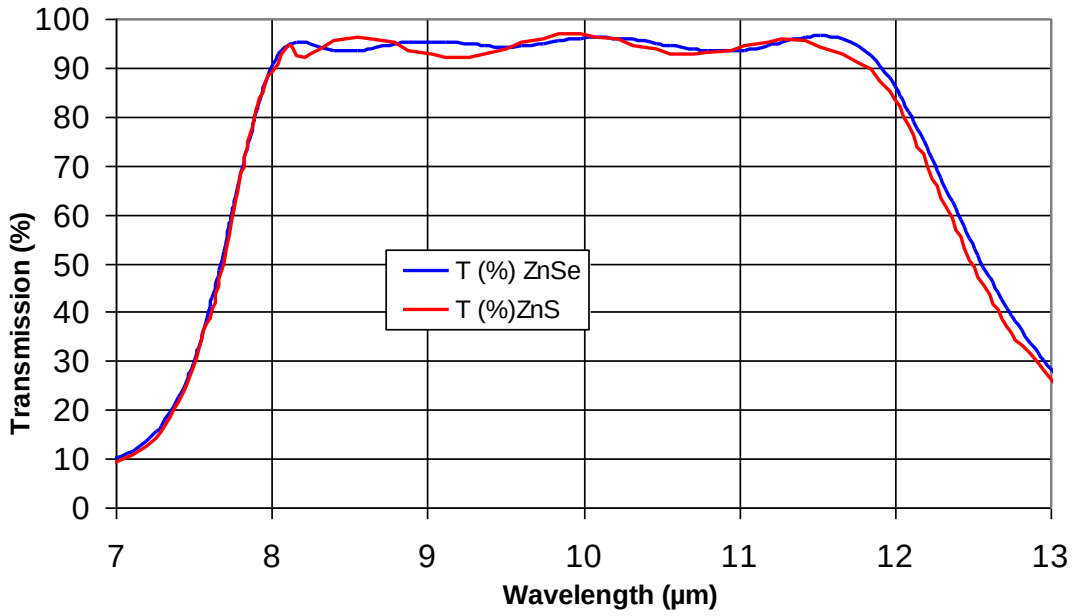

Figure 50. Transmission values for both ZnSe and ZnS.

It is observed that the spectrum of the multilayer coatings realized in this work, were found to be shifted to lower wavelength region as compared to calculated spectra. There could be various reasons resulting from the growth conditions, the source materials used and the nature of the deposition process. One of the most important factors of this shift can be the packing density of the grown layers. As described in Section 3.2, in almost all different kinds of growth techniques, the deposited layers have packing factors less than the ideal value of unity. This causes lower refractive index values and higher absorption than expected in the corresponding wavelength region. Lowering of the refractive index ends up with a shift of the wavelength region for which the transmission is maximum to lower values. This is an expected result since the effective optical thickness is reduced. As a result of necessary calculations we have verified that this is indeed the case for our samples,. In our study, especially for PbTe samples a pronounced shift has been observed. In order to estimate the affect of low packing density on refractive indices we have performed iterative calculations to match produced and calculated multilayer performance. These calculations suggested that a packing density of 0.74 has been realized in our growth conditions for PbTe. Therefore, this value is taken as a reference in all calculations for the designs.

As can be found in the literature there exist several methods to increase the packing density and therefore the refractive index for a better performance [29]. The most common way to increase the packing density is substrate heating and post annealing of the grown structure. The duration and the heating temperature, of course vary with the material, for PbTe on ZnS, temperatures about 175 ºC have been reported to increase the refractive index by modifying the packing factor [29].

Another method that increases the refractive index is the reduction of the carrier concentration of the deposited films. This can be done by several methods like; deposition in oxygen atmosphere, post annealing of the grown structure in air or changing the stoichiometry of the deposition materials [4].

According to Evans and Sally [40] there is a direct relationship between the refractive index and the carrier concentration of the produced films of PbTe. According to Figure 51 the refractive index of deposited PbTe increases with decreasing number of free carriers.

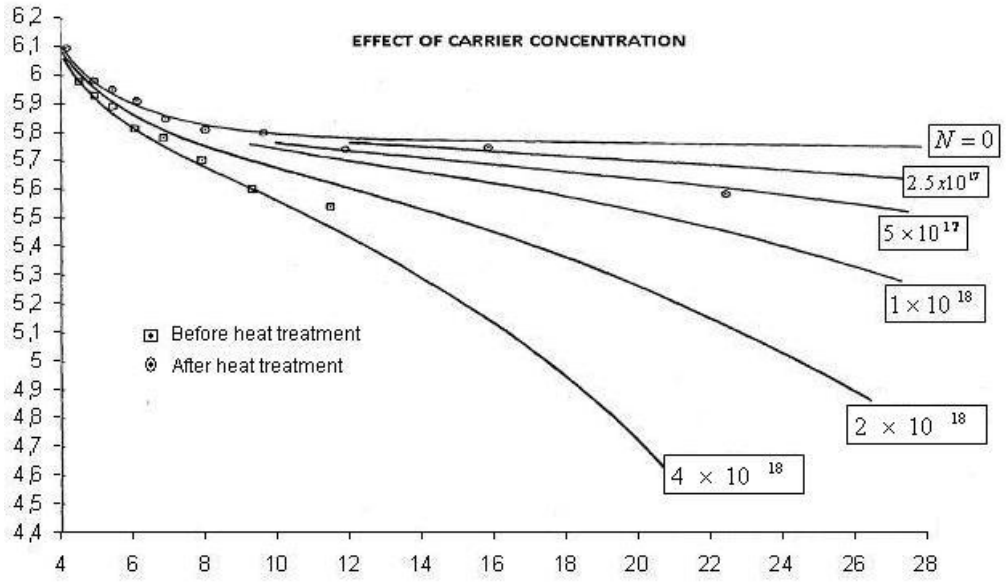

Figure 51. Dispersion curve of PbTe for several carrier concentrations given in cm^{-1} [39].

In addition above explained possible causes of the spectral shift we have observed that small shifts of the peak positions of the transmission curves from the calculated ones seen in

Figures 44 and 47. This could be the result of thickness errors occurring during deposition. The decreasing thickness of ZnSe affects the transmission of the multilayer structure as seen in Figure 52.

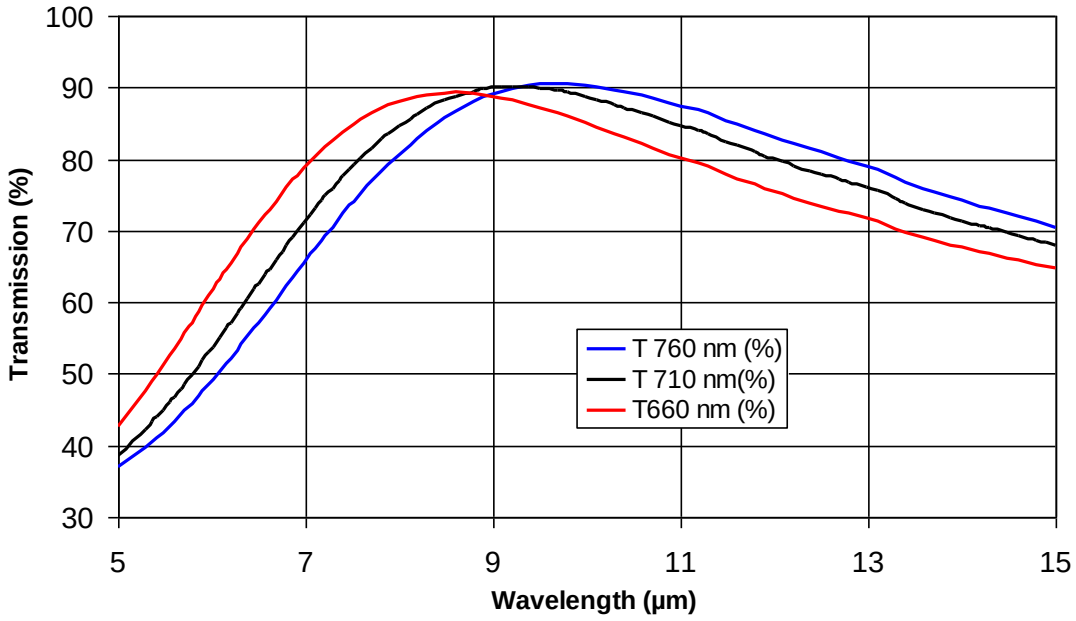

Figure 52. Effect of thickness changes of ZnSe on transmission performance.

According to Figure 52 it is clear that decrease in thicknesses of the ZnSe, shifts the peak position towards shorter wavelengths. We have checked that, this is also true for the other layer material, i.e. PbTe by The Essential Macleod calculations.

In summary, in this thesis work we have produced AR coatings operating at 8-12 µm range where the thermal imaging systems work. The materials used as refractive optical elements in such systems have high reflectance that has to be prevented. We have chosen germanium, zinc sulfide as substrate, lead telluride and zinc selenide as the layer materials. The corresponding coating designs were performed with the help of the commercial thin film calculation program called “The Essential Macleod”. It is found that the various features of this program like material library, packing density modification and optimization give a powerful control on the design processes. PVD Handy Magnetron Sputtering System with RF power supply was preferred since it produces more uniform and stoichiometric films as

compared to other conventional systems like e-beam or thermal evaporation systems. However, in our system, to load the substrates we have to open the whole chamber since we do not have a load lock. Therefore, oxidation of target materials occurs during loading process. Thus, pre-sputtering of targets before opening the shutter is quite necessary to remove the oxide layers on the targets.

In the characterization of substrate materials ellipsometer and FTIR are used. During FTIR measurements, it is observed that the transmittance values may change measurement to measurement depending on the background. Thus, we recommend that after background correction, transmission measurement of a well known sample should be used to check if the measurement conditions are the same. One other critical issue was shown up during the thickness measurement by using Dektak. If the thickness is measured over a relatively long distance, after some point the measured thickness is not indicating the real value due to the changes of the relative orientation of the back of the substrate with respect to the system stage resulting from wedge like irregularities. For a reliable thickness measurement, instead of a single step, consecutive multiple steps must be produced on the sample. To check if there exist any degradation problems in the produced layers, we have compared the two transmission curves obtained in six months intervals from the same sample. It was observed that there was no considerable change in the characteristics.

As a final conclusion; we have achieved our goals in this work. The final products are 3-layer coating, PbTe/ZnSe/PbTe, on ZnS and 2-layer coating PbTe/ZnS on Ge having more than 90% transmittance in 9.7-10.3 μm wavelength region. The realized range is narrower than the aimed one. We have shown that, the method developed in this thesis would yield AR-coatings with broader spectral response if a system having better control on deposition parameters is used.

CHAPTER 5

CONCLUSION

In this thesis work we have aimed to produce AR coatings on Ge, ZnS and ZnSe substrates, operating in 8-12 μm, where the thermal imaging systems work. The coating materials were chosen to be PbTe and ZnSe as high and low index materials, respectively. The coating designs obtained by "The Essential Macleod", the thin film calculation program were found to require at least 7 layers some of which are thicker than a micro meter. Since these thicknesses cannot be realized with sputtering systems, we have narrowed down to design range. The optical characteristics of the substrate materials obtained from FTIR and ellipsometer measurements were used as an input to "The Essential Macleod". The Needle optimization method resulted in 3-layer coating, PbTe/ZnSe/PbTe, on ZnS and 2-layer coating PbTe/ZnS on Ge having more than 90% transmittance in 9.7-10.3 μm wavelength region.

The theoretical designs described above were utilized by PVD Handy magnetron sputtering system. The peak position of the transmittance curve of produced 3-layer coating, PbTe/ZnSe/PbTe, on ZnS was found to be shifted towards to shorter wavelengths. We have concluded that among the various possible causes, the observed shift is most probably due to realized poor packing density of PbTe layers. In theoretical calculations the packing density was assumed to be unity, we have resolved the discrepancy in the transmission peak by adjusting the packing density factor as 0.74. On the other hand, ZnSe grown on Ge, was found to has a packing density value close to unity resulting in best matching transmittance curve with the theoretical one.

Furthermore, we have managed to develop an AR coating design that could be applied to both ZnS and ZnSe. This feature enables us to coat both materials in the same run which is quite cost effective is the mass production is concerned.

As a final conclusion, both the theoretical and experimental work performed throughout this thesis study has enabled us to design and produce multilayer AR coatings with the predicted performance, successfully. The further improvement in performance can be realized with more detailed structural analysis of the grown layers as well as making appropriate modifications in the growth systems.

REFERENCES

[1]Rafael Advanced Defense Systems LTD., www.rafael.co.il, last visited on 5th. August 2009.

[2] Lubezky, J., Ceren, E., *et al*., Applied Optics, **22,** 1828-1831, 1983.

[3] Bloom, L. A., Applied Optics, **20,** 66-73, 1981.

[4] Hawkins, G. J., "Spectral Characterization of Infrared Optical Materials and Filters", PhD. Thesis, The University of Reading, 1998.

[5] Umicore Electro-Optics Material, www.eom.umicore.com, last visited on 13th.August 2009.

[6] Mousa, A.M. and Ponpon, J.P., Eur. Phys. J. Appl. Phys., **34**, 1–5, 2006.

[7] Thelen, A., Design of Optical Interference Coatings, McGraw-Hill, NewYork, 1989.

[8] Dobrowolski, J. A. and Kemp, R. A., Applied Optics, **29,** 2876-2893, 1990.

[9] Tikhonravov, A. V. and Trubetskov, M.K., OSA Technical Digest Series, **17,** 75-77, 1995.

[10] Tikhonravov, A. V., Vestn. Mosk. Univ. Fiz. Astronomiya, **23,** 91-93, 1982.

[11] Baumeister, P., Applied Optics, **34,** 4835-4843, 1995.

[12] Bunshah, R. F., Handbook of Hard Coatings, Elsevier, NewYork, 2000.

[13] Ohring, M., Material Science of Thin Films, 2nd Ed, Academic Press, USA, 2001.

[14] Bunshah, R. F., Handbook of Deposition Technologies for Films and Coatings, 2nd Ed., Noyes Publications, New Jersey, 1994.

[15] Wasa, K., Kitabatake, M. and Adachi, H., Thin Film Materials Technology, Springer, USA, 2004.

[16] Öktem, B., "High Temperature Superconducting $YBa_2Cu_3O_{7-\delta}$ Thin Films and Bolometers", PhD. Thesis, İzmir Institute of Technology, 2006.

[17] Macleod, A. H., Thin Optical Filters, Taylor and Francis, New York, 2001.

[18] Holden, T., www.academic.brooklyn.cuny.edu/physics/holden/, last visited on 9th.August 2009.

[19] Fujiwara, H., Spectroscopic Ellipsometry, Wiley, USA, 2007.

[20] Thermo Nicolet Corp., www.binoybnair.blogspot.com, last visited on 19th.August 2009.

[21] Thin Film Center Inc., Essential Macleod User's Manual, Thin Film Center Inc, USA, 2004.

[22] Welsch, E., Walther, H. G., *et al*., Thin Solid Films, **156,** 1–10, 1988.

[23] Goedicke, K., Liebig, J. S., *et al*., Thin Solid Films, **377-378**, 37-42, 2000.

[24] Laux, S., Richter, W., *et al*., Applied Optics, **35,** 97-101, 1996.

[25] Ogura, S., Sugawara, N., *et al*., Thin Solid Films, **30**, 3-10, 1975.

[26] Kaiser, U., Kaiser, N., *et al*., Thin Solid Films, **217**, 7-16, 1992.

[27] Jerman, M., Qiao, Z., *et al*., Applied Optics, **44,** 3006-3012, 2005.

[28] Khawaja, E., E., Durrani, S., M., A., *et al*., J. Phys. D: Appl. Phys., **36,** 545–551, 2003.

[29] Yen, Y., Zhu, L., *et al*., Applied Optics, **23,** 3597-3601, 1984.

[30] Krishna, M., G., Rao, K., N. and Mohan, S., Proceedings of APCOT 91, Singapore, 1991.

[31] Lia, S., Yang, Y., *et al*., Chinese J. Chemical Phys., **20**, 706-710, 2007.

[32] Harris, M., Macleod, H., A., *et al*., Thin Solid Films, **57**, 173-178, 1979.

[33] Veeco, www.veeco.com, last visited on 17th.August 2009.

[34] Rogatto, D.R., The Infrared and Electro-Optical Systems Handbook, **3**, SPIE Optical Engineering Press & Infrared Information Analysis Center, 1993.

[35] ISP Optics, www.ispoptics.com, last visited on 24th. August 2009.

[36] Rocky Mountain Instrument Co., www.rmico.com, last visited on 24th August 2009.

[37] R. P. Edwin, M. T. Dudermel, and M. Lamare, Applied Optics, **17,** 1066-1068, 1978.

[38] Randall, C. M. and Rawcliffe, R. D., Applied Optics, **6,** 1889-1895, 1967.

[39] Dobrowolski, J., A., Panchhi, P., *et al,* Applied Optics, **35,** 102-105, 1996.

[40] Evans, C., and S., Seely, J., S., Journal de Physique, **29**, 37-42, 1968.